Deformation bands and alteration in porous glass-rich volcaniclastics: Insights from Milos, Greece

E. Leroy, T. Cavailhes, Y. Anguy, R. Soliva, A. Rotevatn, C. Gaborieau

Deformation bands and alteration in porous glass-rich volcaniclastics: Insights from Milos, Greece.

Leroy E., Cavailhes T., Anguy Y., Soliva R., Rotevatn A., and Gaborieau C.

Keywords: Fault, cataclasis, corrosion gulfs, smectites, sealing.

Highlights:

- We document Normal-sense Compactional Shear Bands (NCSBs) in porous volcaniclastics.
- Pumice vesicles are zones of mechanical weakness promoting cataclasis development.
- Glass alteration is expressed by corrosion embayments and smectites neoformation.
- This study details hydraulic self-sealing of NCSBs in the vadose zone.

Abstract:

Deformation bands in porous volcaniclastics are little studied structural heterogeneities despite their relevance for constraining the modalities of deformation development and related fluid-rock interactions in volcanic areas.

We document a dense network of normal-sense Deformation Bands (Normal-sense Compactional Shear Bands (NCSBs) affecting upper Pliocene felsic glassy tuffites in Milos, Greece. NCSBs probably formed between 300 and 500 m of burial depth, in response to NE-SW directed extension which is related to volcanic rift development in the area. They accommodate mm- to m-shear-offsets, trend either N105 ± 10° or N070 ± 10°, and show mutual cross-cutting relations. The NCSB fault rock is made of ultracataclasite in which the cataclastic mechanisms have affected both the mineral fraction and the volcanic glass. Minerals are fractured along their cleavages whereas ~~the~~ pumices are interestingly fractured along their vesicles.

The development of chemical alteration (dissolution and cementation) essentially into the ultracataclasite is expressed through glass-hosted corrosion gulfs and smectites filling the intergranular porosity. These observations support that NCSBs preferentially retained water, have been the seat of greater fluid flow, and are the locus of ongoing phyllosilicate self-sealing in the vadose zone. A significant decrease (up to one order of magnitude) in porosity is measured within the studied NCSBs.

1. Introduction

"Volcaniclastics" is a term introduced by Fisher (1961) to name sedimentary rocks containing at least 10% of volcanic materials. The mechanical deformation (brittle and / or plastic) of porous volcaniclastic rocks (porosity $\Phi > 15\%$) under the effect of tectonic stresses has been poorly documented compared to other porous rocks such as carbonates (e.g. Antonellini et al., 2008; Rotevatn et al. 2016) and clastic sandstones (e.g. Aydin, 1978; Fossen et al., 2007). The diversity of volcaniclastics in terms of mineralogy (i.e. cleaved minerals, volcanic glass, alteration phases) and microstructures (e.g. grain and pore size, shape and angularity) leads to a complex and inhomogeneous mechanical behavior during deformation that deserves to be further described and contextualized through natural examples (Heap and Violay, 2021). Understanding deformation processes, deformation bands (Dbs) and/or fracture occurrence/development and related fluid-rock interactions in volcaniclastics is crucial for investigating fault strength variability (Ikari et al., 2013; Tschegg et al., 2020; Kameda et al., 2019), modalities of volcanic edifice collapse (Evans and Bradbury, 2004; Soden and Shipton, 2013; Blahut et al., 2022), ore deposits and factors controlling their occurrence (Lindsay, 1982), sealing capacities of CO_2-sequestration sites (Annunziatellis et al., 2008) and both geothermal and hydrocarbon reservoirs (Zhu et al., 2011; Schutter, 2003; Zou, 2013). We focus here on small-displacement (millimeter-meter throw) deformation bands and faults cutting porous glass-rich volcaniclastic rocks.

Deformation bands (Dbs) are the most common structural elements related to strain localization in deformed porous granular media (Aydin, 1978; Antonellini and Aydin, 1994; Fossen et al., 2007). They are tabular-planar structures of finite mm-width in which grain sliding, rotation (i.e. granular flow) and/or fracturing (cataclastic flow) act individually or in concert during compaction, dilation and/or shearing processes (e.g. Du Bernard et al., 2002; Fossen et al., 2007).

Dbs have been described in different types of volcaniclastics (Bates and Jackson, 1987) such as non-welded ignimbrites (Wilson et al., 2003; 2006; Riley et al., 2010; Dinwiddie et al., 2012;), basaltic porous tuffs (Okubo, 2014), pumice-rich non-welded tuffs with no devitrification (Evans and Bradbury, 2004) and phenocryst-rich andesitic volcaniclastic sandstones (Lin and Huang, 2014; Cavailhes and Rotevatn, 2018). They have been studied in compressive settings where they exhibit both reverse-sense and strike-slip kinematics (Cavailhes and Rotevatn, 2018) as well as in extensive/transtensional settings where they show normal-sense kinematics (e.g. Evans and Bradbury, 2004; Wilson et al., 2006; Riley et al., 2010). Adopting a kinematics classification, Pure-Compactional Bands (PCB), Pure-Dilation Bands (PDB), Simple Shear-bands (SSB), Compactional Shear-Bands (CSB) and Dilation Shear-Bands (DSB) have all been recognized in such rocks in which high porosities are systematically required for Dbs development (e.g. Dinwiddie et al., 2006; Okubo, 2012; Okubo, 2014; Cavailhes and Rotevatn, 2018). They commonly form at very shallow burial

depths of deformation (Okubo, 2014), from ~ 0.1 km (Okubo, 2012), > 0.2 km (Bradbury and Evans, 2004) to ~ 0.5-1.5 km (Cavailhes and Rotevatn, 2018). They occur as a single strand or anastomosed multi-strand features, preferentially localized into the fault damage zone of both currently active and inactive faults (Dinwiddie et al., 2006; Riley et al., 2010; Okubo, 2012). The degree of welding, the presence of water, the grain nature (glass, mineral, lithophysae), their grain size, shape and structure (e.g. presence of mineralogical cleavages) all have an impact on cataclasis development, related granular flow, and therefore on multi-scale fault-zone architecture (Zhu et al., 2011; Price and Bauer, 1985; Moon, 1993a,b, Okubo, 2012). Such microstructural factors control grain contact areas and geometries responsible for the mechanical response of the rock (microcracks and cataclasis development) to the local stress field (Antonellini and Pollard, 1995; Liu et al., 2021). Deformation in Cataclastic Deformation Bands (CDBs) can be explained by a shear localization preferentially affecting the relatively weak glass phases whereas the magmatic minerals (e.g. plagioclase, pyroxene, amphibole) are less comminuted and therefore considered a strong phase, despite their cleavage planes and inherited microfractures, promoting fracturing and sliding (Wilson et al., 2006; Cavailhes and Rotevatn, 2018). In addition to this observation, well-developed S-C structures within the contractional relays of such CDBs argue for a duality of grain strengths during the deformation (Finch et al., 2020) in shallow burial conditions (0.5-1.5 km). This contribution addresses how the cataclastic deformation does affect porous volcaniclastics that are rich in highly vesiculated pumices. To our knowledge, this point has never been addressed so far.

1.1 Diagenetic alteration

Alteration of volcaniclastics depends upon the interplay between compaction and/or shear-enhanced compaction and fluid-rock interaction, the latter leading to dissolution, neoformation of diagenetic products e.g. phyllosilicates and/or cementation (Mathisen and McPherson, 1991; García-Romero et al., 2005; Allen et al., 2022). Volcanic glass alteration can be overdeveloped into CDBs where the intense comminution along with the resulting increase of the total volumetric surface area of clasts in relation to cataclasis development seems to promote newly-formed mineralogical phases (Wilson et al., 2006).

Numerous factors come into play in the alteration process including Si activity, pH, alkalinity, the activity of alkalis and alkaline earth elements, temperature, pressure and the partial pressure of H_20 (Hay, 1977; Iijima, 1980; Christidis, 2001).

The nature of the diagenetic products strongly depends upon the openness of the diagenetic system. In the one hand, dissolution of unstable volcanic glass may lead to neoformed smectites where the $\frac{(Na^+ + K^+)}{H^+}$ activity is low i.e. where alkalis are leached in a well flushed system (Sheppard and Gude, 1973; Hay, 1977; Dibble and Tiller, 1981; Senkayi et al., 1984; Hay and Guldman, 1987; Christidis and Scott, 1997; Christidis, 1998, 2001; Godelitsas et al., 2010). On the other

hand, a higher ratio of $\frac{(Na^+ + K^+)}{H^+}$ activity, as encountered in semiclosed / closed systems, shall favor formation of alkaline zeolites over that of smectites (Hess, 1966; Sheppard and Gude, 1973; Dibble and Tiller, 1981; Hay and Guldman, 1987).

The required amount of Mg (and perhaps Fe) for smectite formation may be sustainably supplied by the pore fluids (Christidis, 2001), mostly seawater (Godelitsats et al., 2010), or may also be provided by small uptakes from the solid phase and by local migration (Christidis and Dunham, 1997). Smectites can form via a localized *in situ* alteration (replacement) process, via a dissolution/precipitation process including a transport stage or via a translocation process *i.e.* from an external source by colloidal transport (e.g. soil; Wilson et al., 2006). It has been reported for faulted systems that the newly-formed phases require in all cases fluid-rock interactions which can be due to (i) a higher fluid flux into the fault zone than into the host rock (HR) or (ii) a preferential retention of fluids by the fault rock thanks to capillarity processes due to grain-size reduction, such as described in deformed sandstones, poorly lithified sediments and volcaniclastics into the vadose zone (Sigda and Wilson, 2003; Wilson et al., 2006; Cavailhes et al., 2009).

1.2 Petrophysical properties of Dbs and faults in volcaniclastics

With the exception of dilation bands, Dbs in volcaniclastics are systematically characterized by a reduction of porosity relative to the host rock (Dinwiddie et al., 2006; Wilson et al., 2003; Evans and Bradbury, 2004; Lin and Huang, 2014). This is particularly true in CDBs where cataclastic processes can reduce the Db porosity by one order of magnitude compared to host rock (Cavailhes and Rotevatn, 2018).

Despite the work of Okubo (2012) addressing the whole fault zone permeability into porous volcanic tuffs, permeability measurements in individual Dbs have not been published so far. There is no direct, nor simple relationship between (1) permeability, *i.e.* open vs. closed system and (2) porosity and/or pore size. For example, in the vadose zone, in a semiarid to arid climate, low-porosity / small-sized-pore Dbs preferentially retain water and can ultimately be much more permeable than the surrounding host-rock protolith (Wilson et al., 2006). As reported by these authors in non-welded ignimbrites, anastomosed Db strands can act as a true open system and thus represent preferential flow pathways promoting smectite neoformation much more than in the surrounding high-porosity host rock. Such observations of Dbs self-sealing processes e.g., by smectite neoformation, are presently lacking for deformed porous glassy andesitic volcaniclastics.

The objectives of this contribution are (i) to accurately describe an easily accessible “remarkable” outcrop exhibiting spectacular Dbs network in porous volcaniclastics, (ii) to describe the structures and the microstructures of a highly developed Dbs network affecting porous glassy volcaniclastics under a local extensional stress-field, and (iii) to extract the different deformation and alteration

mechanisms (e.g. corrosion and cementation), as well as their controlling factors, leading to the present-day state of the studied deformation features. In addition, we aim (iv) to discuss the poorly documented hydraulic behavior of the Dbs affecting porous volcaniclastics into the vadose zone, and its consequences on self-sealing processes. To address these four original points, we study in detail the so far non-investigated outcrops of Sarakiniko located along the north shore of Milos Island (Greece).

Terrestrial case studies as the current one may also help to document smectite occurrence on extra-terrestrial faulted volcaniclastics (e.g. Mars, Okubo, 2012; Sarhar et al., 2022).

2. Geological setting

The studied area is located in Milos (Cycladic islands, Greece) which is part of the Aegean volcanic arc, which results from the northwards subduction of the African plate underneath the Aegean microplate in an overall convergent setting (Pe and Piper, 1972; Le Pichon and Angelier, 1981; Kassaras et al., 2020). The subduction started ~145 My ago and, since the upper Oligocene (~30 Ma), the position of the magmatic arc has started its southward motion due to slab retreat (Jolivet and Brun, 2010; Ring et al., 2010). A coeval regional back-arc extension started ~30 Ma ago, as expressed by a continental crust thinning across the Aegean Sea (Ring et al., 2010; Jolivet et al., 2021). This crustal thinning results in the development of deep offshore basins bounded by seismogenic faults and a Moho discontinuity located at relatively shallow depths (Anastasakis and Piper, 2005; Nomikou et al., 2014).

The island of Milos is made of four main geological units: (i) the alpine metamorphic basement (Mesozoic in Fig. 1), (ii) the Neogene sedimentary rocks (Upper Miocene – Lower Pliocene in Fig. 1), (iii) the volcanic sequences (Mid Pliocene to upper Pleistocene in Fig. 1) and (iv) the alluvial cover (Recent in Fig. 1) (Sonder, 1924; Fytikas, 1977; Fytikas et al., 1976, 1986; Zhou et al., 2021).

Upper Miocene to early Pliocene volcaniclastic sediments have been nonconformably deposited into WNW-SSE-trending extensional post-orogenic basins overlying the metamorphic basement of the Aegean micro-plate (Mercier, 1981; Van Hinsbergen et al., 2004). Volcanism in the Milos archipelago started subsequently, about 3.5 Ma ago, and has built in concert with tectonic uplifts of the present-day islands (Fytikas et al., 1986; Stewart, 2003; Stewart and McPhie, 2003). The Milos volcanic succession is composed of calc-alkaline volcanics, from basaltic andesite to rhyolite with a predominance of andesites and dacites (Fytikas et al., 1986; Stewart, 2003; Zhou et al., 2021).

Milos is situated within a complex system of crossing neotectonic grabens that can be interpreted as part of 10 km-scale submerged volcanic rifts (Pe-Piper and Piper, 2005; Nomikou et al., 2013; Preine et al., 2022, Fig.1b). Plio-Quaternary deformations are therefore complex, multi-directional, partly synchronous, cross-

cutting, seismogenic, and subjected to volcanism (Fytikas, 1989; Papanikolaou et al., 1993; Kokkalas and Aydin, 2013). The alluvial cover is mainly deposited in these structurally-controlled depressions.

- During the Pliocene, NE-SW extension has been described by Jarrigue, 1978).
- Late Pliocene NW-SE extension was expressed along ENE striking faults systems (Angelier, 1979; Mercier, 1981; Phase I in Kokkalas and Aydin, 2013).
- During the lower Pleistocene (noted "Calabrian" (1.8; 0.8 Ma) in Mercier, 1981), an unconformable sedimentation in Milos has been described and tentatively related to a lower Quaternary poly-directional compressional event recognized in the back-arc domain (Angelier, 1977; Jarrigue, 1978; Mercier, 1981).
- During the Middle to the Upper Pleistocene, a N-S directed faulting/fracturing event is consistent with an E-W direction of extension in both onshore and offshore domains of Milos (Mercier, 1981; Anastasakis and Piper, 2005; Kokkalas and Aydin, 2013). Simultaneously, the NW-SE trending Vromolimni-Kondaro fault bounding the western side of the Milos gulf has showed a strong tectonic activity, triggering upper Pleistocene hydrothermal circulations (Liakopoulos et al. 2001).
- A clear Quaternary reactivation of the existing NW-SE normal faults has been described by Angelier (1979). This NW-SE-trending network of normal faults is likely responsible for the current-day physiography of Milos, in particular the NW-SE elongation of its gulf, along the Vromolimni-Kondaro fault. This NE-SW direction of extension is also consistent with the one derived from the focal mechanisms of 1987's earthquakes at shallow depths, which were aligned along the NW-SE graben (1-10 km; Ochmann et al. 1989). The studied Pierre fault (see section 4.3) appears subparallel and probably contemporaneous to these structures. Positive geothermal anomalies are clearly associated with the Plio-Quaternary structural heterogeneities which localize and favor the hydrothermal circulation (Angelier, 1977; Fytikas, 1989, Ochmann et al., 1989). Surprisingly, the GPS-derived horizontal velocity across Milos is perfectly N-S directed with a velocity of 2.66 mm yr^{-1} (Bohnhoff et al., 2006).

2.4 Sarakiniko geology

The studied area is located along the northern shoreline of Milos and includes a crowded touristic white cove called Sarakiniko beach (Figs. 1b and 2). The morphology of the white-colored coastline displays sharp, jagged and irregular morphologies leading to N-S elongated and dissected coves, 10 m-deep canyons and drowned erosional features (erosional meanders) that are characteristics of a fractured and rapidly submerging area (Figs. 2 and 3a).

Sarakiniko's volcaniclastic porous rocks are part of the upper Pliocene tuffites succession previously described as shallow-water-reworked acid/felsic tuffs

exhibiting porous sandstones and conglomerates, composed of pumiceous clasts usually up to 15 cm in diameter, rarely 50 cm, and a fine glassy matrix of ash or sand (Fytikas et al., 1977; Stewart and McPhie, 2003). The studied porous rocks are overlain by up to 30 m–thick Quaternary reworked porous tuffs made of reddish fine volcanic materials that can be locally fossiliferous (Fytikas et al., 1977). These poorly-consolidated volcaniclastic sediments which have been filling pre-existing N-S canyons, have therefore smoothened the coastal morphologies before being incised by the present-day erosion (Figs. 2 and 3a).

Based on the structural cross-sections displayed in work by Fytikas (1977), the maximum burial depth of the studied Upper Pliocene porous tuffs could have reached 450 m at Sarakiniko, mainly due to Quaternary andesitic lava dome settlement.

3. Methodology

A multi-scale structural analysis was conducted nearby the Sarakiniko beach in 2021/2022. Structural bedding dips, faults, fractures, and Dbs have been mapped and studied using satellite images, drone imagery and detailed fieldwork. The attributes of the structural heterogeneities have been measured *in situ* (*i.e.*, strike, dip, thickness, length, spacing and connectivity; e.g. Fig. 3a).

Rock sampling was oriented with respect to measured structural bedding dip. Db samples (13 samples for 21 thin-sections) have been carefully collected and oriented according to their strike, dip and slip vector, the latter being inferred from local bedding offset. The collected samples were subsequently dried during 48 hours before impregnation using an epoxy resin. The samples were cut along the X-Z deformation axes plan containing the slip vector (Cavailhes et al., 2014). Petrographic and microstructural analyses were performed using an optical microscope and a scanning electron microscope (SEM) on representative thin-sections. The SEM was an environmental ThermoFisher/FEI QUANTA 250 FEG (I2M, France). Observations were made in a low vacuum of 75 to 100 Pa using low to moderate acceleration voltage and beam current. Electronic micrographs were acquired either in secondary electron (SE) mode (topographical contrast) or in backscattered electron (BSE) mode (phase contrast). Elemental analysis and chemical/mineralogical characterizations were done by X-ray Energy Dispersive Spectrometry (X-EDS) using an integrated EDAX spectrometer. X-EDS characterization of the mineral/grain fraction was complemented by optical Raman spectroscopy using a Renishaw/INVIA Raman micro spectrometer fitted with a 785 nm monochromatic laser wavelength.

Local porosity values were estimated based on the analysis of SEM micrographs of representative Db thin sections. Image analysis involved binarization of grey-level SEM images (e.g. Torabi et al., 2015), using a standard image processing platform (ImageJ) and following a similar workflow as that of Rotevatn et al. (2016). For each thin-section, local porosity estimations were made within Dbs and in the adjacent host rock (HR). The size l of the local sliding

window over which porosity was measured is a function of grain size and of the width of the structure for Dbs. In the HR, the characteristic size l of the local measurement window was 1.5 mm versus 0.5 mm in Dbs. Measured local porosity values were last averaged in the HR, and in the Dbs, over sub centimetric-wide bands normal to the Db/HR boundary and ~10 times wider than the size of the measurement window, which allowed to quantify local porosity dispersion.

4. Results

4.1 Structural lineaments mapping

From Mandrakia to Konstantinos, the northern shoreline of Milos displays dissected and jagged coastal morphologies related to the presence of three main sets of structural discontinuities, expressed by structural lineaments (e.g. Sander et al., 2007 for mapping limitations). The latter were mapped using aerial picture analysis and partly calibrated with field structure orientation measurements (Fig. 2a). Upper Pliocene strata show 5 to 20° eastwards bedding dips.

(i) The main structural pattern is given by NW-SE striking lineaments (spatial deviation ~ 090 – 130°, Fig. 2b) which do not exhibit any clear spatial clustering (Fig. 2a). Fault slip analysis around Mandrakia and east of Sarakiniko reveals striations consistent with N-S to NE-SW extension (Fig. 2a). Interestingly, this set of lineaments seems to display a slight change of direction at Sarakiniko, striking ~ 090 (Figs. 2a and 3a). The orientation of the Sarakiniko fault could be either related to the spatial deviation of NW-SE structural trend and/or to unknown < 100 m-scale structural complexities leading to local stress rotation.

(ii) A nearly N-S (~ 015) striking structural fabric is also observed all over the area. This second set has a less pervasive geomorphologic expression than the previous set. This direction seems to control both the incision and the filling related to Q.tv volcaniclastic deposition (Fytikas, 1977).

(iii) A third trend expressed by sharp NE-SW structural lineaments (~ 045-070) is locally identifiable through the western peninsula of Konstantinos nearby Pachena, as well as in the eastern Mandrakia Peninsula (Fig. 2).

At the 100 m-scale of investigation represented in Fig. 2, the three aforementioned sets cut the studied Upper Pliocene succession whereas only both of the NW-SE and N-S sets seem to cut the Quaternary deposits previously mapped as Q.tv by Fytikas (1977). A detailed field structural analysis shows that locally in Sarakiniko (Fig. 3b), the NE-SW fractures crosscut the others, i.e. they have clearly postdated both the E-W (belonging to set (i) above) and the N-S trending networks of structures.

4.2 Host rock characterization

The depositional environment of the Upper Pliocene tuffs has been successfully investigated by Stewart and McPhie (2003). A detailed lithologic log of the Sarakiniko tuffs is provided in this study (Fig. 3c) in order to (i) estimate the shearing displacement of the faults / Dbs cutting the relatively homogeneous studied formation, and to (ii) characterize any possible lithological control on deformation style, type and occurrence.

The studied Upper Pliocene volcaniclastic interval is ~22 m -thick and dips ~10-15° eastwards (Figs. 3a and 3c). It is made of bedded, graded and laminated porous sandstones and conglomerates, composed of pumiceous clasts wrapped into a fine glassy matrix of grey to white ashes or sand (Fig. 3d). Three m-thick intervals are relatively massive and exclusively made of grey ashes exhibiting m-scale chaotic ball and pillow structures, such as commonly described for seismites (Montenat et al., 2007; at 5 m, 17 m, and 20 m in Fig. 3c). These layers (labelled in Fig. 3a) have a notable geomorphologic consequence at Sarakiniko in partly shaping cuestas. An anisopac greenish layer composed of fine sand and ashes constitutes a reliable marker for estimating fault and Dbs offsets (at 4-5 m on Fig. 3a and labelled GL in Fig. 3c). This layer has been mined and excavated along the western cliff of the Sarakiniko canyon.

The studied volcaniclastics are mainly composed of acidic volcanic glass shards (10-50 µm-scale) which aggregate in mm-scale clasts, mm to cm-sized vesiculated pumices (Figs. 3d and 4), and phenocrysts of infra-mm-sized feldspars. There is no post-depositional welding of glass shards (Stewart and McPhie, 2003).

4.3 Structural geology of Sarakiniko

The studied Dbs are part of a 100 m - spaced normal fault network including (amongst others) from north to south, the Chaos fault (CF), the Sarakiniko fault (SF) and the Canyon fault (Fig. 3a). The SF is an E-W trending structure that crosses and slightly shapes the Sarakiniko natural cove as expressed by fractured concave shorelines in its middle part (Fig. 3a). The SF dips southwards approximately ~ 70° and shows ~ 12 meters of estimated normal displacement. Such displacement was estimated from stratigraphic correlation, in particular by investigating the vertical displacement between the two fault blocks hosting the GL stratigraphic marker (Figs. 3a and 3c).

The SF fault damage zone, in the sense of Caine et al. (1996), is expressed by N090 to 130 NW-SE striking clusters of Dbs and appears relatively symmetrical in its northern and southern fault blocks (Figs. 3a and 3e). The hanging wall fault block hosts the Sarakiniko Canyon where numerous Dbs and clusters of Dbs with cm to m-offsets displace among others the GL stratigraphic marker (Fig. 3e; cross-section B-B'). Synthetic and antithetic Db clusters are spaced by meters to tens of meters and define m-scale to 10 m-scale systems of horsts and grabens. The density of Dbs ~~is~~ slightly increases from south to north, starting 40 m away

from the SF (Fig. 3e). This area is therefore defined as the SF outer wall damage zone (Choi et al., 2016).

The footwall of the SF exhibits numerous homogeneously distributed clusters of 070-120 striking Dbs. Occurrence of brittle fractures appears limited to the vicinity of the SF fault (Fig. 3a). Dbs density does not clearly increase towards the SF at the 10 m -scale (Figs. 3c and 3e).

The following is a characterization of Pierre Fault located 10 meters further north from the SF. –The Pierre fault can be interpreted as either part of the SF damage zone or as part of the background fracturing (Figs. 3a, 3e and 4a). Indeed, as other authors e.g. Wilson et al. (2006) and Cavailhes and Rotevatn (2018), we aim to characterize and understand incipient deformation processes and related alteration on a m-offset cluster of Dbs cutting volcaniclastics.

4.4 Macrostructural analysis of Pierre fault Dbs network (Sarakiniko)

Dbs at Sarakiniko are light-colored tabular structures accommodating mm- to m-shear-offsets (Fig. 4a; e.g. Fossen et al., 2007) and dissecting the porous volcaniclastic succession. They are in positive relief compared to surrounding volcaniclastic rocks, most likely in response to their higher resistance to weathering (Fig. 4b).

The Dbs trend either N105 ± 10° or N070 ± 10°, dip both northwards and southwards, and have mutual cross-cutting relations, therefore supporting their contemporaneous development (Fig. 4a). The spacing between structures ranges from 10's of centimeters to meters.

The Dbs occur either as individual strand or multi-strand clusters (up to 10 cm in thickness) of anastomosing bands (Fig. 4b). On the one hand, Dbs of a given set can rotate in the vicinity of another set of Dbs, therefore appearing parallel and branched to the latter. On the other hand, the Dbs of a given set can simply be crosscut by another set (Fig. 4a). Both antithetic and synthetic structures are recognized for both Db sets, the smaller structures tending to connect the major ones (Fig. 4a).

The Db segment lengths are 1 to 5 meters, individual strand lengths being usually lower than 3 meters (Fig. 4a). Clusters of Dbs can be hundreds of meters long (Fig. 3a).

Single Db shear-displacement ranges from millimeter to centimeter whereas Dbs cluster shear-displacement, such as recognized in the studied Pierre fault, can reach more than 1 meter (133 cm; Figs. 4a and b). Qualitatively, the thicker and longer is the structure (Db or cluster of Db), the more important is the shear-offset on this structure (Figs. 3e and 4a).

Single Db or clusters of Dbs at Sarakiniko do not exhibit clear striation such as reported in other porous volcaniclastics (e.g. Cavailhes and Rotevatn, 2018). Some slight grooves have been tentatively interpreted as slickensides, without any clear and conclusive evidence for it. This point will be discussed further below.

4.5 Microstructural analysis of the Db samples (Sarakiniko, Pierre fault)

The m-displacement Pierre fault exhibits cm-thick deformation band fault rock bounded by sharp sliding planes (Fig. 4c). Grain-size reduction is visible in the Db compared with the surrounding host rock (HR), at both the outcrop and the sample-scale (Figs. 4b and 4c). Volcanic glass clasts within the Db appear more greywhite, more angular, crushed and comminuted by intragranular and intergranular fracturing than in the surrounding host rock (Fig. 4c). Yet, some of the clasts seem to retain the protolith initial grain-size (Fig. 4c). Grains within the Db are predominantly volcanic glass grains. The surrounding rock is slightly fractured without any clear kinematical relation with the deformation architecture into the band (Fig. 4c). Sparse iron oxide-hydroxide grains of about 500 µm are located both inside and outside the Db (Fig. 4c). These oxides-hydroxides are not significantly fractured in comparison to the glass grains, suggesting that mineralization postdates glass fracturing.

Generally speaking, the Db fault rock is exclusively made of ultracataclasite in the sense of Nogueira et al. (2021) i.e. more than 90% of the Db fault rock shows a grain-size significantly smaller than 1 mm (Figs. 4c and 5a).

4.5.1 Mechanical deformation

Deformation of vesiculated pumices

At the vicinity of the Dbs, the angle between fractures and the elongated vesicles in pumices can be either low (Figs. 5a and b) or high (Fig. 5c).

In the first case (Fig. 5a), a cm-scale pumice clast (HR side) exhibits a volcanic fabric typified by ~500 µm-long ellipsoidal vesicles. The vesicles are slightly rotated along the Db/HR shear-plane without any clear fracturing and shearing such as described for convex normal drag fold (Fig. 5a; Brandes and Tanner, 2014). Grain-size reduction is clearly recognized across the sharp Db/HR shear-plane boundary (Fig. 5a). The pumice clasts in the Db show grain-sizes in the range 10 - 500 µm versus a cm-size in the HR (Fig. 5a). The quite varied orientation of the elongated vesicles of the small-sized Db pumice clasts (which contrasts with the uniform orientation on the HR side) strongly supports that they have been rotated (Fig. 5a). The reddish color into the Db is probably explained by iron oxides (Fig. 5a). SEM microstructural analysis shows that µm-scale shearing can occur between subparallel vesicles, leading to a kind of extensional relay expressed by dense fractures and related micro-clast genesis (Fig. 5b). The newly-formed clasts appear mechanically incorporated into the band (Fig. 5b).

In the second case (Fig. 5c), synthetic and antithetic shear-fractures offset the vesicles of a cm-scale pumice clast in the HR side at the vicinity of a Db. The fractures are spaced by less than 1 mm and are connected to the main Db volume. Grain-size reduction is also recognized into the Db and demonstrates the damage-zone development by grain fracturing (Fig. 5d). Density and connectivity of both intra-granular and transgranular fractures increase in the vicinity of the Db (Fig. 5d), such as commonly reported in brittle fault rock development (Zhu et al.,

2011). Interestingly, the volcanic glass displays µm-hemispheric gulfs (Fig. 5d) suggesting alteration processes that are described and discussed further below.

Deformation of plagioclases

In cross-polarized light, plagioclase phenocrysts appear fractured and crushed in the vicinity of the Db (Fig. 6a). This results in a decrease of mineral grain size along the Db which is typified by communited µm-sized dragged (mechanically incorporated) clasts (Figs. 6b and 6c). Near the Db edge, angles between the fractures are around 70°, some of them display µm-shear-displacements (Figs. 6b and 6c). Fractures seem preferentially located along plagioclase cleavage planes and localize the shearing displacement (Fig. 6c).

4.5.2 Fluid-rock interaction, alteration and neoformed phases (diagenesis)

In the studied cataclastic Db fault rocks, SEM-micrographs taken in Dbs e.g. Fig. 7a reveal the common occurrence of honeycomb-shaped (rigid bladed plates) neoformed minerals filling the intergranular porosity (e.g. Fig. 7b) or, less frequently, coating volcanic glass shards (e.g. Fig. 7c). X-ray EDS spectra acquired locally over the honeycomb-shaped-material are essentially compatible with the generic stoichiometry of dioctahedral smectites (e.g. Fig. 7d).

A HR/Db boundary is illustrated in the SEM micrograph provided in Fig. 7e. As shown by the X-EDS chemical mapping provided in Fig. 7f, the Db shows a clear enhancement in magnesium (Mg) compared to the HR-side (i.e. the brighter the yellow color, the higher the concentration (At%). Mg-enrichment in the Db is obviously related to the filling of the intergranular porosity (and the coating of comminuted volcanic glass clasts to a lesser extent) by neoformed smectites (e.g. Figs. 7b and 7c).

Neoformed smectites are far less prevalent in the HR compared to Dbs. In the HR, smectites can be found only locally in the form of large plates coating glass grains (Fig. A1.A) and/or fresh reactive surfaces (Fig. A1.B). In contrast to Dbs, smectites are not found in the HR as a secondary cement filling the intergranular porosity.

SEM micrographs reveal also the common occurrence of corrosion (hydration) as micron-sized hemispheric gulfs on volcanic glass shards in the sense of Knight et al. (2000) (Figs. 8a and 8b). These corrosion embayments are either isolated or coalescent (Figs. 7a, 7c and 8a-b). In some rare instances, the floor of these embayments can show slight traces of smectite (Fig. 8b).

Halite crystals can be locally found in Db areas where the intergranular porosity is filled with neoformed smectite (Fig. 8b). EDS chemical mapping highlights massive halite cementation along some Db/HR boundaries, HR side (Figs. 8c and 8d). The halite cement clearly seals the intergranular porosity in the HR. The µm-sized cubic-shaped halite crystals do not display any fractures. This cementation event obviously postdates Dbs formation (Fig. 8d).

Sub-millimeter porous pumices dissolved to varying degrees and locally coated with smectite can be observed within single strand Dbs or in between Db strands (e.g. Figs. 8e and 8f).

4.6 Dbs porosity

The SEM micrographs collected in this study reveal a significant loss of porosity within the Dbs which have accommodated ~ 1 m or ~ 1 cm of shear-offset (Fig. 9). Host rock values range from 16 to 33%. Db porosity values for m-offset are comprised between 2 and 3% against 4 to 6% for cm-offset. These values are consistent with those reported for cm-offset cataclastic Dbs in volcaniclastics showing reverse and strike-slip kinematics (Cavailhes and Rotevatn, 2018; Fig. 9).

In Dbs, porosity is mainly associated with intragranular pores such as previously described for vesiculated pumices (e.g. Fig. 5a), intergranular pore space related to cataclasis as well as structural porosity in the form of more or less connected intra-granular and transgranular fractures (e.g. Figs. 5 and 6). These distinctive features therefore introduce a structurally-driven porosity anisotropy in the studied rocks.

5. Discussion

Dbs in Sarakiniko are conjugated tabular structures of mm- to cm-scale width in which cm- to m-shear displacements are generally accommodated by each single strand (Aydin, 1978; Fossen et al. 2007). Based on the measured low porosity within the Dbs (Fig. 9), their kinematics (Fig. 4a), their microstructural characteristics (i.e. the presence of cataclasis, Fig. 6b) and according to the terminology used in work by Aydin et al. (2006), the studied Dbs are hereafter referred to as Normal-sense Compactional Shear Bands (NCSB). These NCSBs clearly accommodate a combination of compaction and shear, by means of grain crushing, grain fracturing and cataclasis, aided by grain reorganization/disaggregation.

5.1 Normal-sense Compactional Shear Bands and the geology of Milos

The porous volcaniclastics of the Sarakiniko formation hosting the studied NCSBs are Upper Pliocene in age (1.85 – 1.8 my) (Fytikas, 1977; Stewart, 2003). The network of structural heterogeneities (that has been built by NW-SE-trending NCSBs) is clearly top-sealed by a major unconformity and the subsequent alluvial Quaternary deposits which are labelled Q.tv on the geological map of Fytikas (1977) (Figs. 2 and 3). These observations suggest that the NE-SW-directed extension responsible for the NCSBs formation occurred at the transition between the Late Pliocene and the Earliest Quaternary, as suggested for the phase I described in the figure 4 of Angelier (1979). The studied NW-SE trending NCSBs are clearly postdated by N-S trending brittle-style fracturing (Fig. 3b). The N-S

brittle fracturing event would be associated with the Middle to Upper Pleistocene extension described in Mercier (1981) and in the tectonic phase 2 mentioned in Kokkalas and Aydin (2013).

These two types of features associated with two different deformation events are respectively subparallel to the NW-SE Milos gulf graben and the N-S quaternary Zephyria graben (Fig. 1); they can therefore be seen as part as two overlapping damage zones which are located between two diachronous volcanic rifts. The studied ~N110-trending Db network is almost perpendicular to the nearest part of the subduction trench and could be seen as a simple back arc-extension (Brun et al., 2016) or as a wing-like extensional quadrant of the major Mid Cycladic Lineament (Kokkalas and Aydin, 2013). Nevertheless, these inferences do not explain the presence of the 5 km-scale N-S trending Zephyria graben (Fig. 1b). This simple observation severely complicates the geometry of the system where multi-striking, crossing and imbricated volcanic rifts have been simultaneously actives in the recent times (Fytikas, 1977).

Particularly along the E-W Sarakiniko fault (SF), the top-sealing Q.tv tuffs display a slight NW-SE brittle fracturing pattern, although they are porous (Figs. 2 and 3a). The SF, mainly associated with NCSBs development at the end of the Late Pliocene, also cuts the Quaternary deposits (Q.tv) and does exhibit a brittle deformation style made of open fractures (Fig. 3b). In addition, the Sarakiniko fault (SF) crosscuts the Dbs network and seems to have a limited post Quaternary normal displacement < 3 m (Fig. 3). The aforementioned facts do suggest that the SF has been slightly reactivated during the recent times (late Quaternary), as suggested by its sharp fault trace along the northern shore of Milos; remarkably, this last fault movement did not reactivate the surrounding studied NCSBs network (Fig. 4a).

5.2 Network architecture

The studied Pierre fault is made of a cluster of NCSBs affecting porous volcaniclastics (Fig. 10a). This cm-thick cluster is part of a background pattern of synthetic and antithetic Dbs that are located between 10 m-offset normal faults (Fig. 3). The synoptic diagram in Fig. 10a highlights the sub-seismic scale of our study (< 20 m) where NCSBs are numerous, conjugated, and clearly undetectable using both conventional and high-resolution seismic data (e.g. Faleide et al., 2021). Indeed, a simple transect perpendicular to the 10 m-offset faults would cross tens of the structural heterogeneities that have been described in this manuscript (Figs. 3 and 10a).

Both the high frequency of NCSBs and the high connectivity of the network suggest that these tectonic structures must be taken in account in quantifying reservoir fault-seal properties, as previously demonstrated in siliciclastic sandstones (e.g. Fisher and Knipe, 1998; Davatzes, 2003).

5.3 Deformation mechanisms

5.3.1. Cataclasis, burial depth and shear-displacement

In clastic sandstones, the formation of Dbs is strongly pressure-sensitive (Mair et al., 2002); when Dbs formed, increasing burial depth generally promotes cataclasis (e.g. Fossen et al., 2007). In addition, both the shear displacement and shear magnitude induce and enhance cataclasis development in Dbs even at low confining stress conditions (e.g. Mair et al., 2002; Rotevatn et al., 2008; Ballas et al., 2015). Pizzatti et al. (2020) have shown that particulate flow predates and conditions cataclasis development during increasing shear-displacement, in particular by reducing the initial porosity of the fault rock to 5-6%.

In porous mineral-rich volcaniclastics and for a similar range of burial depth of deformation, Cavailhes and Rotevatn (2018) have shown that compactional shear bands exhibit cataclasis whereas pure compaction bands (PCBs) do not. The shearing process seems *de facto* necessary for cataclasis development without excluding a burial depth control. Indeed, the transition depth from granular flow to cataclastic flow would be located at ~ 300 ± 100 m for fragile tuffitic components (Beke et al., 2019). Frictional sliding concentrates on discrete fault planes at the margin of Cataclastic Deformation Bands (CDBs) or along a fracture plane at ~500 ± 100 m of burial depth during deformation in volcaniclastics (Beke et al., 2019).

At Sarakiniko, observations show that the last stage of normal faulting crosscutting the Q.tv Quaternary deposits did not generate any NCSB within the studied Upper Pliocene succession in near-surface conditions of deformation (Fig. 3a). Instead, open fractures developed whereas (i) the high porosity of the host rock and (ii) the shear displacement associated with normal faulting were respectively still present and effective. Based on these facts and neglecting the possible variability in kinetics of mechanical deformation during the two distinct deformation events, we suggest that burial depth is also a critical parameter to form and effectively develop cataclasis in deformed porous glassy volcaniclastics (Fig. 10b). In addition, cataclastic flow has also been recognized into the Dbs with mm-shear-displacement, therefore suggesting that particulate flow would not be a precursor to cataclasis development, in contrast to porous arkosic clastics (Pizzati et al., 2020).

5.3.2 Inferring the burial depth during deformation

Deformation processes can be used to determine the range of depths in which the studied NCSBs developed. This is particularly true for porous volcaniclastics in extensional settings (Beke et al., 2019). Given the presence of cataclasis into the Sarakiniko NCSBs, we can consider that the burial depth of deformation was higher than 300 m ± 100 m, the depth at which cataclastic mechanisms become effective in these lithologies. This range of burial values is slightly shallower than the one previously proposed for cataclasis development in porous mineral-rich volcaniclastics under a transpressive regime (Cavailhes and Rotevatn, 2018), but still consistent with CDB observed in highly porous sandstones (Soliva et al., 2013). Using an independent approach, this depth of deformation (300 m ± 100

m) would be consistent with the possible eroded overlying rock thickness inferred from the cross-sections provided with the geological map of Fytikas (1977).

5.3.3 Mechanical contrasts in the host volcaniclastics

Minerals vs glass deformation.

The minerals in the studied volcaniclastic sandstones (essentially plagioclase phenocrysts) are fractured along mineralogical cleavages, therefore promoting mechanical deformation along these natural mechanical weaknesses (Fig. 10b; e.g. Cavailhes and Rotevatn, 2018). Owing to cleavage-guided-fractures, these minerals are subsequently sheared and dragged into the NCSBs (Figs. 6b and 6c). The feldspars are not altered in contrast with the volcanic glass (Fig. 6).

The volcanic glass is crushed at the vicinity of the NCSBs by connected and conjugated planes of brittle fractures (Fig. 5d). The increase of both the density and connectivity of these fractures, as well as an increase in shear displacement along these fractures lead to cataclasis development towards the edge of the NCSB (Fig. 10b). Fracturing of glass grains also leads to pore collapse. Deformation therefore uses the initial pore spaces for grain reorganization by granular flow. Along that line, the particular rheology of pumices can lead to vesicle collapse at very shallow depth (tens of meters), reducing the pore volumes more than the volcanic glass (Peterson, 1979).

Cataclastic flow within NCSBs is therefore promoted by mechanical 2D weaknesses (cleavage planes) within the mineralogical phenocryst fraction and a bulk weakness associated with the glass fraction and its intra-grain porosity (vesicles); contribution from the pumice vesicles has been certainly overlooked in the literature. The glass fraction being here far more important than the phenocryst fraction (mainly plagioclases) cataclasis is more intense than in phenocrysts-rich porous materials, and probably self-sustained.

Striation and S-C structures

Surprisingly, slickensides along the NCSBs surfaces are absent at Sarakiniko, whereas very-well expressed striation and S-C structures have been reported along the Shihtiping Cataclastic Shear-Compaction Bands in Taiwan (Cavailhes and Rotevatn, 2018).

In our case study, the absence of well-defined striation during NCSB development is consistent with distributed shearing expressed by both granular and cataclastic flow (Fossen et al., 2007); the transition from cataclastic flow to brittle faulting (generating discrete fault planes) therefore did not occur (Wong et al., 1997; Rotevatn et al., 2008). The significant shear offset observed on the studied structures (e.g. 1.33 m at the Pierre fault; Figs. 4 and 10a) is surprisingly even more important that the one reported for the aforementioned Shear Compaction Bands of Taiwan; this ~~fact~~ suggests an offset-independent mechanism for striation occurrence. This difference in rheological style is most likely related to compositional differences in HR mineralogy, differences of burial depth during deformation and/or a non-evaluated difference in stress-ratio during

deformation (Angelier, 1989; Philit et al., 2019). Indeed, the porous volcaniclastics studied here are essentially glassy. This composition constitutes a major difference compared to work by Cavailhes and Rotevatn (2018) in which phenocrysts were more abundant. Brittle deformation and striation development at Sarakiniko were restricted to the surrounding 10 m-offset main faults (sensu Ramsay, 1967) (Fig. 3).

S-C structures have not been recognized at Sarakiniko. This suggests that the surrounding rocks did not macroscopically accommodate any rock-mass deformation. This duality/variability in deformation styles between Taiwan and Milos may simply be related to the high abundance of glass at Sarakiniko, in contrast to the numerous phenocrysts recognized at Shihtiping. Indeed, the rheology is notably controlled by the relative percentage of mechanical "strong" phases in comparison to the glassy "weak" phase, therefore promoting S-C structures development in Taiwan (Finch et al., 2020 for numerical modelling).

5.4 Fluid-rock interactions

5.4.1 Chronology of the alteration

The neoformed phyllosilicates, essentially smectites, are not deformed, compacted, reshaped or sheared by (i) the faulting phases and/or (ii) cataclasis development (e.g. Figs. 7c and 10b). Smectites exhibit pristine honeycomb morphologies, which suggests that phyllosilicate formation postdates cataclasis (Figs. 7b, 8b and 10b). Given the weak stability of volcanic glass, we propose that the deformation stage (cataclasis in NCSBs) occurred early during the geological history of the studied volcaniclastics, and was followed by a later alteration.

5.4.2 Spatial distribution of alteration

Both hydration / corrosion gulfs (i.e. the dissolution of Si) and neoformed smectites are preferentially observed within the NCSBs, (Fig. 7f) where pores are smaller than in the host rock. As smectite neoformation requires fluid(s)-rock interactions, this supports that NCSBs preferentially retained water and have been the seat of greater fluid flow (Wilson et al., 2006). Such a situation is expected in the vadose zone (i.e. two-phase flow) of semiarid climates (Sigda and Wilson, 2003; Wilson et al., 2006) as in the case of the studied formation.

In addition, the ubiquitous addition of smectites, and the absence of zeolites, in NCSBs support that the pore fluids acted as a sink in NCSBs, which have been accordingly well flushed (Hess, 1966; Mariner and Surdam, 1970; Hay, 1977; Dibble and Tiller, 1981; Senkayi et al., 1984; Steefel and van Cappellen 1990; Christidis and Scott, 1997; Christidis, 1998, 2001; Godelitsas et al., 2010).

In NCSBs, smectites are essentially observed as a cement filling some of the intergranular voids (e.g. Figs. 7b and 8b) irrespective of the location of corrosion

713 gulfs which are basically void of any smectite[1]. We consistently see smectite-free
714 hydration embayments on glass shards and cementitious smectite in some of the
715 intergranular voids. In some locations, hydration gulfs are present and the
716 intergranular porosity is smectite-free. This suggests (1) dissolution of volcanic
717 glass in NCSBs and (2) smectite addition are spatially and temporally decoupled
718 events, the former preceding the latter. This obviously implies a transport stage
719 between dissolution of the glass at hydration gulfs e.g. $(SiOH)^{\circ}_{4(aq)}$ (Kamei et al.,
720 2000) and smectite addition in intergranular voids. Seawater was most likely the
721 vector for transport as supported by NaCl crystals located in NCSBs (e.g. Fig. 8b)
722 and its direct proximity (Fig. 3). Thus, alteration and subsequent local filling of
723 intergranular voids by smectite occurred most likely in a submarine environment
724 in an open system as reported elsewhere at Milos (Christidis, 1998) (at depth, the
725 groundwater is the seawater). Alteration involved leaching of alkalis and Si
726 (dissolution of the volcanic glass by the reaction with seawater) along with an
727 uptake of Mg (may be Fe also) from seawater (Godelitsas et al., 2010) flowing
728 preferentially through NCSBs (Wilson et al., 2006). Smectites precipitated
729 subsequently in local zones where the vadose fluid was supersaturated cf e.g.
730 through evaporation of seawater.

731 More marginally, smectites in NCSBs can form *in-situ* during the dissolution
732 of the volcanic glass or more precisely, at the expense of the volcanic glass,
733 probably through a poorly crystalline Si-rich allophane precursor cf e.g. Fig. 7c,
734 which may be paralleled to Figure 7 in Christidis (2001). In this latter case,
735 smectites coat altered glass shards and shall be viewed as pore-lining smectites vs.
736 pore-filling smectites in the more general case described above.

737 In the HR, typified by much larger pore dimensions, the alteration looks quite
738 different from that prevailing in NCSBs. Corrosion embayments are basically
739 absent and smectite addition is observed in some rare local areas in the form of
740 large plates coating glass grains and/or fresh reactive surfaces (Fig. A1 in
741 Appendix A). This suggests that (within the vadose zone of semiarid climate) the
742 HR remained essentially dry due to unfavorable pore size. Of course, this main
743 trend does not exclude that locally within the HR, the volcanic glass could be
744 temporarily in contact with essentially non-flowing water. In this situation,
745 comparable to a local closed to semi-closed system, Na and K are, as always, first
746 depleted (White, 1983) and smectites can form *in-situ* during the early stages of
747 alteration onto weathered glass surfaces (Fig. A1 in Appendix A)[2] (as
748 occasionally seen within NCSBs e.g. Fig. 7c, in more open chemical and
749 hydrologic conditions). As the residence time of water pockets in the HR is
750 limited due to evaporation (as expressed e.g. by halite cementation in Figs. 8c and
751 8d), high ratios of $\frac{Na^+ + K^+}{H^+}$ activity could not be reached in the basically non-

[1] Only in some rare instances e.g. Fig. 8b, the floor of a corrosion embayment can include slight traces of smectites.

[2] In such *closed or semiclosed microenvironments*, random ripening of smectite might also have occurred (Christidis, 2001).

752 flowing water pockets and zeolites did not postdate smectites within the rare HR
753 closed microenvironments.

754 Alteration of the sub-mm porous pumices that can be seen in NCSBs may be
755 viewed as a compromise between the end-members alteration situations discussed
756 above i.e. NCSBs vs. HR. Highly dissolved materials (Fig. 8e) are clear evidence
757 of enhanced fluid fluxes episodes that typify NCSBs while occurrence of pore-
758 lining smectites (Fig. 8f) is more typical of HR porosity dimensions and water to
759 rock ratio. See also Fig. A2 in Appendix A.

760 **5.5 Normal-sense Compactional Shear Bands and reservoir properties**

761 The loss of porosity into the studied Normal-sense Compactional Shear Bands
762 (NCSBs) is clearly related to cataclastic mechanisms and pore collapse leading to
763 enhanced close-packing of grains that are reduced in size (Figs. 9 and 10b).
764 NCSBs porosity is one order of magnitude smaller than in HR (Fig. 9), which is
765 much more significant than porosity reductions previously reported in other types
766 of Dbs in volcaniclastics (Dinwiddie et al., 2006, 2012; Wilson et al., 2003; Evans
767 and Bradbury, 2004; Lin and Huang, 2014).

768 On the one hand, the high connectivity of the NCSB network (Fig. 10a), the
769 common cm-to dm- NCSB cluster thickness, and the significant and systematic
770 loss of porosity associated with ultracataclasite development, support that these
771 "sub-seismic scale" faults shall act as preferential subsurface water pathways in
772 the vadose zone of semiarid climate (network connectivity e.g. Shipton and
773 Cowie, 2001; Shipton et al., 2005; vadose zone i.e. Wilson et al., 2006). In other
774 words, the studied NCSB network shall act as capillarity conduits as described in
775 sandstones (Sigda and Wilson, 2003: Cavailhes et al., 2009; Balsamo et al., 2012)
776 and volcaniclastic tuffs (Wilson et al., 2006). As discussed above, this most likely
777 explains preferential addition of pore-filling smectites within the low porosity
778 ultracataclasites rather than within the host rock.

779 Evolution of these conductive NCSBs can lead to enrichment in pore-filling
780 phyllosilicates, which is ultimately expected to decrease the permeability of these
781 fault-zones (e.g. Yielding et al., 2002; Kaproth et al., 2010; Lommatzsch et al.,
782 2015). Self-sealed ultracataclasite NCSBs may therefore finally act as seawater
783 barriers which may play a role in the NaCl cementation, HR side, seen in Figs. 8c-
784 d. This observation may be paralleled to bucket effects described in sandstones for
785 iron oxides localization (Eichhubl et al., 2004; Cavailhes et al., 2009). Another
786 candidate explanation for the halite cementation illustrated in Figs. 8c-d is that
787 seawater that preferentially resides in flows through NCSBs in the vadose zone of
788 semiarid climate spills out of the ultracataclasite channels, HR side along
789 HR/NCSB boundaries, where it gets trapped due to unfavorable pore size for two-
790 phase flow (e.g. Lux and Anguy, 2012), and ultimately evaporates leading to
791 halite cementation.

792 The above hydrological inferences on NCSBs appear crucial for assessing
793 fractured porous volcaniclastic subsurface reservoirs associated with buried

794 volcanoes (e.g. Bischoff et al., 2017) and characterizing fault self-sealing
795 properties in geothermal reservoirs in which hydrous weathering and neoformed
796 phyllosilicates are prone to compartmentalize fluid flow (Fytikas et al., 1989).

797

798

799 **6. Conclusions**

800 The present study documents:

801 - A dense network of Dbs classified according to their petrophysical and
802 structural characteristics as Normal-sense Compactional Shear Bands
803 (NCSBs) affecting porous felsic glassy volcaniclastics; NCSBs formed at
804 shallow depth, probably between 300 and 500 m.
805 - The deformation is consistent with the damage-zones of polyphased
806 volcanic rifts in Milos. The main faults have been reactivated during the
807 Quaternary whereas the NCSBs network was not, probably in response to
808 shallower conditions of burial (i.e. near-surface conditions) during this
809 latter event.
810 - Cataclastic mechanisms do affect both the mineral fraction (essentially
811 plagioclase) and the volcanic glass (shards and pumices).
812 - Development of alteration (dissolution and cementation) through
813 corrosion gulfs and honeycomb-shaped smectites in NCSBs.
814 - Mineralogical and elemental differentiations between HR (host rock) and
815 NCSBs suggest NCSBs preferentially retained water and have been the
816 seat of greater fluid flow.
817 - A significant decrease (up to one order of magnitude) in porosity is
818 measured within the studied NCSBs.

819 This study provides an example of ongoing phyllosilicate self-sealing of
820 ultracataclasites in volcaniclastics in the vadose zone of semi-arid climates (i.e.
821 two-phase flow).

822 **Acknowledgements**

823 This research was partly supported by the INSU funding of the CNRS (Centre
824 National de la Recherche Scientifique). We wish to thank P. Mosser for
825 recognizing the area before the COVID-19 lockdown. O. Chazot, A. Safarikas, H.
826 Gillet and V. Hanquiez are acknowledged for providing drone and satellite images
827 of Milos and Sarakiniko. We thank M. Saint-George and M.-C. Perello for
828 technical assistance. We thank J-E. Martelat, S. Augier, P. Grandjean, L. Maigne,
829 V. Breton, L. Terray, P. Chardon, J. Escartin, P. Nomikou, K. Bejelou for field
830 assistance and scientific discussions. M. Pizzati, the anonymous reviewer and the
831 editor of JSG, T. Takeshita, are sincerely acknowledged for their constructive
832 comments on the initial version of this manuscript.

833 **References:**

Allen, S. M., Marsaglia, K. M., Morgan, J., & Franco, A. (2022). Origin and diagenetic priming of a potential slow-slip trigger zone in volcaniclastic deposits flanking a seamount on the subducting plate, Hikurangi margin, New Zealand. New Zealand Journal of Geology and Geophysics, 65(1), 179-200.

Anastasakis, G., and Piper, D. J. (2005). Late Neogene evolution of the western South Aegean volcanic arc: sedimentary imprint of volcanicity around Milos. Marine Geology, 215(3-4), 135-158.

Angelier, J., 1977. Sur l'évolution tectonique depuis le Miocène supérieur d'un arc insulaire méditerranéen : l'arc Ogden. Rev. Geogr. Phys. G&01. Dyn., (2), 19 (3): 271-274.

Angelier, J., 1979. Recent Quaternary tectonics in the Hellenic Arc: examples of geological observations on land. In: C.A. Whitten, R. Green and B.K. Meade (Editors), Recent Crustal Movements, 1977. Tectonophysics, 52: 267-275.

Angelier, J. (1989). From orientation to magnitudes in paleostress determinations using fault slip data. Journal of structural geology, 11(1-2), 37-50.

Annunziatellis, A., Beaubien, S.E., Bigi, S., Ciotoli, G., Coltella, M., Lombardi, S., 2008. Gas migration along fault systems and through the vadose zone in the Latera caldera (central Italy): implications for CO2 geological storage. Int. J. Greenh. Gas Control 2, 353–372.

Antonellini, M., Aydin, A., 1994. Effect of faulting on fluid flow in porous sandstones: petrophysical properties. AAPG Bull. 78, 355–377.

Antonellini M. A. and Pollard D. D. 1995. Distinct element modeling of deformation bands in sandstone. Journal of structural Geology 17(8), 1165-1182.

Antonellini, M., Tondi, E., Agosta, F., Aydin, A., Cello, G., 2008. Failure modes in deep water carbonates and their impact for fault development: Majella Mountain, Central Apennines, Italy. Mar. Petrol. Geol. 25 (10), 1074–1096.

Aydin, A., 1978. Small faults formed as deformation bands in sandstone. Pure Appl. Geophys. 116, 913–930.

Aydin, A., Borja, R.I., Eichhubl, P., 2006. Geological and mathematical framework for failure modes in granular rock. J. Struct. Geol. 28 (1), 83–98. http://dx.doi.org/10.1016/j.jsg.2005.07.008.

Ballas, G., Fossen, H., & Soliva, R. 2015. Factors controlling permeability of cataclastic deformation bands and faults in porous sandstone reservoirs. Journal of Structural Geology, 76, 1-21.

Balsamo, F., Storti, F., Gröcke, D., 2012, Fault-related fluid flow history in shallow marine sediments from carbonate concretions, Crotone basin, south Italy: Journal of the Geological Society, London, v. 169, p. 613–626, doi:10.1144/0016-76492011-109.

Bates, R. L., & Jackson, J. A. 1987, Glossary of geology

Beke, B., Fodor, L., Millar, L., and Petrik, A. (2019). Deformation band formation as a function of progressive burial: Depth calibration and mechanism change in the Pannonian Basin (Hungary). Marine and Petroleum Geology, 105, 1-16.

881 Bischoff, A. P., Nicol, A., and Beggs, M. (2017). Stratigraphy of architectural
882 elements in a buried volcanic system and implications for hydrocarbon
883 exploration. Interpretation, 5(3), SK141-SK159.
884 Blahůt J., Mitrovic-Woodell I., Baroň I., René M., Rowberry M., Blard P.
885 Hartvich, F., Balek, J. and Meletlidis S. (2020). Volcanic edifice slip
886 events recorded on the fault plane of the San Andrés Landslide, El Hierro,
887 Canary Islands. Tectonophysics 776, 228317.
888 Bohnhoff, M., Rische, M., Meier, T., Becker, D., Stavrakakis, G., and Harjes, H.
889 P. (2006). Microseismic activity in the Hellenic Volcanic Arc, Greece,
890 with emphasis on the seismotectonic setting of the Santorini–Amorgos
891 zone. Tectonophysics, 423(1-4), 17-33.
892 Brandes, C., & Tanner, D. C. (2014). Fault-related folding: A review of kinematic
893 models and their application. Earth-Science Reviews, 138, 352-370.
894 Brun, J. P., Faccenna, C., Gueydan, F., Sokoutis, D., Philippon, M., Kydonakis,
895 K., & Gorini, C. (2016). The two-stage Aegean extension, from localized
896 to distributed, a result of slab rollback acceleration. Canadian journal of
897 earth sciences, 53(11), 1142-1157.
898 Caine, J. S., Evans, J. P. and Forster, C. B. (1996). Fault zone architecture and
899 permeability structure. Geology, 24(11), 1025-1028.
900 Cavailhes, T., Soliva, R., Benedicto, A., Loggia, D., Schultz, R. A., & Wibberley,
901 C. A. J. (2009, September). Are cataclastic shear bands fluid barriers or
902 capillarity conduits? Insight from the analysis of redox fronts in porous. In
903 2nd EAGE International Conference on Fault and Top Seals-From Pore to
904 Basin Scale 2009 (pp. cp-136). EAGE Publications BV.
905 Cavailhes, T., Labaume, P., Sizun, J. P., Soliva, R., Gout, C., Potdevin, J. L.,
906 Buatier, M., Gay, A., Chauvet, A., Charpentier, D. & Trave, A. (2014).
907 Difference in petrophysical properties between foliated and dilatant fault
908 rocks in deeply buried clastics: The case of the Gres d'Annot Formation,
909 SW French Alps. *Terra Nova*, *26*(4), 298-306.
910 Cavailhes T. and Rotevatn A. 2018. Deformation bands in volcaniclastic rocks –
911 Insights from the Shihtiping tuffs, Coastal Range of Taiwan. Journal of
912 Structural Geology 113, 155-175.
913 Choi, J. H., Edwards, P., Ko, K., and Kim, Y. S. (2016). Definition and
914 classification of fault damage zones: A review and a new methodological
915 approach. Earth-Science Reviews, 152, 70-87.
916 Christidis G. E. 1998. Comparative study of the mobility of major and trace
917 elements during alteration of an andesite and a rhyolite to bentonites, in
918 the islands of Milos and Kimolos, Aegean, Greece. Clays Clay Miner. 46,
919 379–399.
920 Christidis G. E. 2001. Formation and growth of smectites in bentonites: a case
921 study from Kimolos Island , Aegean, Greece. Clays and Clay Minerals
922 49(3), 204–215.
923 Christidis G., Dunham A. C. 1993. Compositional variations in smectites: Part I.
924 Alteration of intermediate volcanic rocks. A case study from Milos Island,
925 Greece. Clay Minerals 28, 255-273.
926 Christidis G. and Dunharn, A. C. 1997. Compositional variations in smectites:
927 Part II. Alteration of acidic precursors. A case study from Milos Island,
928 Greece. Clay Minerals 32, 253–270.

Christidis G. E. and Scott P. W. 1997. The origin and control of colour of white bentonites from the Aegean islands of Milos and Kimolos, Greece. Miner. Deposita 32, 271–279.

Davatzes, N. C. (2003). Fault architecture as a function of deformation mechanism in clastic rocks with an emphasis on sandstone. Stanford University.

Dibble W. E. Jr and Tiller W. 1981. Kinetic model of zeolite paragenesis in tuffaceous sediments. Clays Clay Miner. 29, 323–330.

Dinwiddie, C.L., Bradbury, K.K., McGinnis, R.N., Fedors, R.W., Ferrill, D.A., 2006. Fault zone deformation overprints permeability of nonwelded ignimbrite: chalk Cove fault, bishop tuff, bishop, California. Vadose Zone J. 5 (2), 610–627. http://dx.doi.org/10. 2136/vzj2005.0062.

Dinwiddie, C.L., Bradbury, K.K., McGinnis, R.N., Stillman, D.E., Ferrill, D.A., 2012. Hydrogeologic heterogeneity of faulted and fractured Glass Mountain bedded tuffaceous sediments and ash-fall deposits: the Crucifix site near Bishop, California. Lithosphere 4 (1), 40–62. http://dx.doi.org/10.1130/L179.1.

Du Bernard, X., Eichhubl, P., & Aydin, A. (2002). Dilation bands: A new form of localized failure in granular media. Geophysical Research Letters, 29(24), 29-1.

Eichhubl, P., 2004. Paleo-fluid flow and deformation in the Aztec sandstone at Valley of Fire, Nevada. Evidence for the coupling of hydrologic, diagenetic, and tectonic processes, GSA.

Evans, J.P., Bradbury, K.K., 2004. Faulting and fracturing of non-welded Bishop tuffs, eastern California: deformation mechanisms in very porous materials in the vadose zone. Vadose Zone J. 3 (2), 602–623. http://dx.doi.org/10.2123/3.2.602.

Faleide, T. S., Braathen, A., Lecomte, I., Mulrooney, M. J., Midtkandal, I., Bugge, A. J., and Planke, S. (2021). Impacts of seismic resolution on fault interpretation: Insights from seismic modelling. Tectonophysics, 816, 229008.

Finch, M. A., Bons, P. D., Steinbach, F., Griera, A., Llorens, M. G., Gomez-Rivas, E., ... & de Riese, T. (2020). The ephemeral development of C′ shear bands: A numerical modelling approach. Journal of Structural Geology, 139, 104091.

Fisher, R. V. (1961). Proposed classification of volcaniclastic sediments and rocks. Geological Society of America Bulletin, 72(9), 1409-1414.

Fisher, Q. J. and Knipe, R. (1998). Fault sealing processes in siliciclastic sediments. Geological Society, London, Special Publications, 147(1), 117-134.

Fossen, H., Schultz, R.A., Shipton, Z.K., Mair, K., 2007. Deformation bands in sandstone: a review. J. Geol. Soc. 164 (4), 755–769. http://dx.doi.org/10.1144/0016-76492006- 036.

Fytikas, M., 1977, Geological Map of Greece: Milos Island: Athens, Greece, Institute of Geology and Mining Research (IGMR), mapped during the years 1971–1973, scale 1:25,000.

975 Fytikas, M., 1989, Updating of the geological and geothermal research on Milos
976 Island: Geothermics, v. 18, no. 4, p. 485–496, doi:10.1016/0375-
977 6505(89)90051-5.
978 Fytikas, M., Giuliani, O., Innocenti, F., Marinelli, G., and Mazzuoli, R., 1976,
979 Geochronological data on recent magmatism of the Aegean Sea:
980 Tectonophysics, v. 31, no. 1-2, p. T29–T34, doi:10.1016/0040-
981 1951(76)90161-X.
982 Fytikas, M., Innocenti, F., Kolios, N., Manetti, P., Mazzuoli, R., Poli, G., Rita, F.,
983 and Villari, L., 1986, Volcanology and petrology of volcanic products
984 from the island of Milos and neighboring islets: Journal of Volcanology
985 and Geothermal Research, v. 28, no. 3-4, p. 297–317, doi:10.1016/0377-
986 0273(86)90028-4.
987 García-Romero, E., Vegas, J., Baldonedo, J. L., & Marfil, R. (2005). Clay
988 minerals as alteration products in basaltic volcaniclastic deposits of La
989 Palma (Canary Islands, Spain). Sedimentary Geology, 174(3-4), 237-253.
990 Gautier, P., Brun, J. P., & Jolivet, L. (1993). Structure and kinematics of upper
991 Cenozoic extensional detachment on Naxos and Paros (Cyclades Islands,
992 Greece). Tectonics, 12(5), 1180-1194.
993 Godelitsas A., Gamaletsos P. and Roussos-Kotsis M. 2010. Mordenite-bearing
994 tuffs from Prassa quarry, Kimolos island, Greece. Eur. J. Mineral 22, 797–
995 811.
996 Hay R. L. 1977. Geology of zeolites in sedimentary rocks. Pp. 53-64 in:
997 Mineralogy and Geology of Natural Zeolites (E. A. Mumpton, editor).
998 Reviews in Mineralogy, 4. Mineralogical Society of America, Washington,
999 D.C.
1000 Hay R. L. and Guldman S. G. 1987. Diagenetic alteration of silicic ash in Searles
1001 lake, California. Clays and Clay Minerals 35, 449–457.
1002 Heap, M. J., & Violay, M. E. (2021). The mechanical behaviour and failure
1003 modes of volcanic rocks: a review. Bulletin of Volcanology, 83(5),
1004 33.Hess P. C. 1966. Phase equilibria of some minerals in the K20-Na20-
1005 AI203-SiOz-H20 system at 25°C and 1 atmosphere. Am. J. Sci. 264, 289–
1006 309.
1007 Hess P. C. 1966. Phase equilibria of some minerals in the K_20-Na_20-AI_20_3-SiO_2-
1008 H_20 system at 25° C and 1 atmosphere. Am. J. Sci. 264, 289–309.
1009 Iijima A. 1980. Geology of natural zeolites and zeolitic rocks. Proceedings of the
1010 5th International Conference on Zeolites, pp. 103–118.
1011 Ikari M. J., Hüpers A. and Kopf A. J. 2013. Shear strength of sediments
1012 approaching subduction in the Nankai Trough, Japan as constraints on
1013 forearc mechanics. Geochemistry, Geophysics, Geosystems 14(8), 2716-
1014 2730.
1015 Jarrigue, J-J, 1978, Etudes néotectoniques dans l'arc volcanique Egéen: Les îles
1016 de Kos, Santorin et Milos.
1017 Jolivet, L., and Brun, J. P. (2010). Cenozoic geodynamic evolution of the Aegean.
1018 International Journal of Earth Sciences, 99(1), 109-138.
1019 Jolivet, L., Menant, A., Roche, V., Le Pourhiet, L., Maillard, A., Augier, R., Do
1020 Couto, D., Gorini, C., Thinion, I., and Canva, A. (2021). Transfer zones in
1021 Mediterranean back-arc regions and tear faults. Zones de transfert dans les

domaines arrière-arc méditerranéens et déchirures des panneaux plongeants. Bulletin de la Société Géologique de France, 192(1).
Kameda, J., Uno, M., Conin, M., Ujiie, K., Hamada, Y., & Kimura, G. (2019). Fault weakening caused by smectite swelling. Earth, Planets and Space, 71(1), 1-7.
Kamei G., Yusaa Y. and Arai T. (2000). A natural analogue of nuclear waste glass in compacted bentonite. Applied Geochemistry 15, 141-155.
Kaproth, B.M., Cashman, S.M., and Marone, C., 2010, Deformation band formation and strength evolution in unlithified sand: The role of grain breakage: Journal of Geophysical Research: Solid Earth, v. 115, p. 1–11, doi:10.1029/2010JB007406.
Kassaras, I., Kapetanidis, V., Ganas, A., Tzanis, A., Kosma, C., Karakonstantis, A., Valkaniotis, S., Chailas, S., Kouskouna, V. and Papadimitriou, P. (2020). The new seismotectonic atlas of Greece (v1. 0) and its implementation. Geosciences, 10(11), 447.
Knight, J. A., Burger, K., and Bieg, G. (2000). The pyroclastic tonsteins of the Sabero Coalfield, north-western Spain, and their relationship to the stratigraphy and structural geology. International Journal of Coal Geology, 44(3-4), 187-226.
Kokkalas, S., and Aydin, A. (2013). Is there a link between faulting and magmatism in the south-central Aegean Sea?. Geological Magazine, 150(2), 193-224.
Le Pichon, X. and Angelier, J., The Aegean Sea. Philosophical Transactions of the Royal Society of London. Series A, Mathematical and Physical Sciences, 1981, vol. 300, no 1454, p. 357-372.
Liakopoulos, A., Glasby, G. P., Papavassiliou, C. T., and Boulegue, J. (2001). Nature and origin of the Vani manganese deposit, Milos, Greece: an overview. Ore Geology Reviews, 18(3-4), 181-209.
Lin S.-H. and Huang, W.-J. 2014. Study of Deformation Bands in Ignimbrites in Shihtiping, Eastern Taiwan. AGU fall meeting, pp. T31C–T4625 abstract.
Lindsey, D. A. (1982). Tertiary volcanic rocks and uranium in the Thomas Range and northern Drum Mountains, Juab County, Utah (No. 1221). USGPO,.
Liu Z., Fu X., Deng S., Meng L., Wang H., Sun Y. and Chen Z. 2021. The critical control of arkosic sandstone porosity on deformation band formation: Insights from the Shulu across-fault borehole in the Bohai Bay Basin, China. Journal of Structural Geology 143, 104258.
Lommatzsch, M., Exner, U., Gier, S., & Grasemann, B. (2015). Structural and chemical controls of deformation bands on fluid flow: Interplay between cataclasis and diagenetic alteration. Aapg Bulletin, 99(4), 689-710.
Lux, J., & Anguy, Y. (2012). A study of the behavior of implicit pressure explicit saturation (IMPES) schedules for two-phase flow in dynamic pore network models. Transport in porous media, 93(1), 203-221.
Pe, G.G., & Piper D. J. W. (1972). Vulcanism at subduction zones: the Aegean area. ηφαιστειότης εις ζώνας καταδύσεως: η περιοχή του Αιγαίου. Δελτίον της Ελληνικής Γεωλογικής Εταιρίας, 9(2), 132-144.
Mair, M., Elphick, S.C. and Main, I.G., 2002a. Influence of confining pressure on the mechanical and structural evolution of laboratory deformation bands. Geophys. Res. Lett. 29. http://dx.doi.org/10.1029/2001GL013964.

Mariner R. H and Surdam R. A. 1970. Alkalinity and formation of zeolites in saline alkaline lakes. Science 170, 977–980.

Mathisen, M. E. & McPherson, J. G. 1981. Volcaniclastic deposits: implications for hydrocarbon exploration. In: FISHER, R. V. & SMITH, G. A. (eds) Sedimentation in volcanic settings. Society of Economic Paleontologists and Mineralogists, Special Publications, 45, 27-36.

Mercier, J. L. (1981). Extensional-compressional tectonics associated with the Aegean Arc: comparison with the Andean Cordillera of south Peru-north Bolivia. Philosophical Transactions of the Royal Society of London. Series A, Mathematical and Physical Sciences, 300(1454), 337-355.

Montenat, C., Barrier, P., & Hibsch, C. (2007). Seismites: An attempt at critical analysis and classification. Sedimentary Geology, 196(1-4), 5-30.

Moon, V., 1993a. Microstructural controls on the geochemical behaviour of ignimbrite. Eng. Geol. 35, 19–31. http://dx.doi.org/10.1016/0013 7952(93)90067-M.

Moon, V., 1993b. Geotechnical characteristics of ignimbrite: a soft pyroclastic rock type. Eng. Geol. 35, 33–48. http://dx.doi.org/10.1016/0013-7952(93)90068-N.

Nogueira, F. C. C., Nicchio, M. A., Balsamo, F., Souza, J. A. B., Silva, I. V. L., Bezerra, F. H. R., Vasconcelas, D.L. and Carvalho, B. R. B. M. (2021). The influence of the cataclastic matrix on the petrophysical properties of deformation bands in arkosic sandstones. Marine and Petroleum Geology, 124, 104825.

Nomikou, P., Papanikolaou, D., Alexandri, M., Sakellariou, D., and Rousakis, G. (2013). Submarine volcanoes along the Aegean volcanic arc. Tectonophysics, 597, 123-146.

Nomikou, P., Papanikolaou, D., Tibaldi, A., Carey, S., Livanos, I., Bell, K. L. C., Pasquarè, F.A., and Rousakis, G. (2014). The detection of volcanic debris avalanches (VDAs) along the Hellenic Volcanic Arc, through marine geophysical techniques. In Submarine Mass Movements and Their Consequences (pp. 339-349). Springer, Cham.

Ochmann, N., Hollnack, D. and Wohlenberg, J., (1989). Seismological exploration of the Milos geothermal reservoir, Greece. Geothermics, 18(4): 563–577.

Okubo, C.H., 2012. Spatial distribution of damage around faults in the Joe Lott Tuff Member of the Mount Belknap Volcanics, Utah: A mechanical analog for faulting in pyroclastic deposits on Mars. J. Geophys. Res. 117, E08003. http://dx.doi.org/10. 1029/2012JE004105.

Okubo, C. H. (2014). Brittle deformation and slope failure at the North Menan butte tuff cone, eastern Snake River plain, Idaho. Journal of volcanology and geothermal research, 278, 86-95.

Papanikolaou ->Παπανικολάου, Δ., Λέκκας, Ε. Λ., Συσκάκης, Δ., & Αδαμοπούλου, Ε. (1993). Correlation on neotectonic structures with the geodynamic activity in Milos during the earthquakes of March 1992. Δελτίον της Ελληνικής Γεωλογικής Εταιρίας, 28(3), 413.

Pavlides, S., Tsapanos, T., Zouros, N., Sboras, S., Koravos, G., & Chatzipetros, A. (2009, October). Using active fault data for assessing seismic hazard: a case study from NE Aegean sea, Greece. In Earthquake geotechnical

engineering satellite conference XVIIth international conference on soil mechanics & geotechnical engineering (Vol. 10, p. 2009).
Pe-Piper, G., and Piper, D. J. W. (2005). The South Aegean active volcanic arc: relationships between magmatism and tectonics. In Developments in Volcanology (Vol. 7, pp. 113-133). Elsevier.
Peterson, D. W. (1979). Significance of the flattening of pumice fragments in ash-flow tuffs.
Philit, S., Soliva, R., Ballas, G., Chemenda, A., & Castilla, R. (2019). Fault surface development and fault rock juxtaposition along deformation band clusters in porous sandstones series. *AAPG Bulletin*, *103*(11), 2731-2756.
Preine, J., Karstens, J., Hübscher, C., Nomikou, P., Schmid, F., Crutchley, G. J, Druit, T.H. and Papanikolaou, D. (2022). Spatio-temporal evolution of the Christiana-Santorini-Kolumbo volcanic field, Aegean Sea. Geology, 50(1), 96-100.
Price, R.H., Bauer, S.J., 1985. Analysis of the elastic and strength properties of Yucca Mountain tuff, Nevada. In: Ashworth, E. (Ed.), Proceedings of the 26th U.S. Symposium on Rock Mechanics. A. A. Balkema, Rotterdam, Netherlands, pp. 89–96.
Ramsay, J.G., 1967. Folding and Fracturing of Rocks. McGraw-Hill, New York 429pp.
Riley, P.R., Goodwin, L.B., Lewis, C.J., 2010. Controls on fault damage zone width, structure, and symmetry in the Bandelier Tuff, New Mexico. J. Struct. Geol. 32 (6), 766–780. http://dx.doi.org/10.1016/j.jsg.2010. 05.005.
Ring, U., Glodny, J., Will, T. and Thomson, S. (2010). The Hellenic subduction system: high-pressure metamorphism, exhumation, normal faulting, and large-scale extension. Annual Review of Earth and Planetary Sciences, 38(1), 45-76.
Rotevatn, A., Fossen, H., Torabi, A. and Braathen, A., 2008. Slipped deformation bands – a new type of cataclastic deformation bands in Sinai, Suez Rift, Egypt. J. Struct. Geol. 30, 1317–1331.
Rotevatn, A., Thorsheim, E., Bastesen, E., Fossmark, H.S.S., Torabi, A., Sælen, G., 2016. Sequential growth of deformation bands in carbonate grainstones in the hangingwall of an active growth fault: implications for deformation mechanisms in different tectonic regimes. J. Struct. Geol. 90, 27–47. http://doi.org/10.1016/j.jsg.2016.07.003.
Sarkar, S., Bose, N., Bhattacharya, S., & Bhandari, S. (2022). Identification of smectites by IR and LIBS instruments of Super Cam Suite onboard Mars 2020 Perseverance rover: comments on the Non-retrieval of First Drill Core. CURRENT SCIENCE, 123(1), 93.
Sakellariou, D., & Tsampouraki-Kraounaki, K. (2016). Offshore faulting in the Aegean Sea: A synthesis based on bathymetric and seismic profiling data. Bulletin of the Geological Society of Greece, 50(1), 134-143.
Sander, P. (2007). Lineaments in groundwater exploration: a review of applications and limitations. *Hydrogeology journal*, *15*(1), 71-74.
Schutter, S.R., 2003. Hydrocarbon occurrence and exploration in and around igneous rocks. In: Petford, N., McCaffrey, K.J.W. (Eds.), Hydrocarbons in Crystalline Rocks, vol. 214 Geological Society, London, Special Publications pp. 7-33.

Senkayi A. L., Dixon J. B., Hossner L. R., Abder-Ruhman M. and Fanning, D. S. 1984. Mineralogy and genetic relationships of tonstein, bentonite and lignitic strata in the Eocene Yegna Formation of East-Central Texas. Clays and Clay Minerals 32, 259–271.

Sheppard R. A. and Gude A. J. 1973. Zeolites and associated authigenic silicate minerals in tuffaceous rocks of the Big Sandy Formation, Mohave County, Arizona. U.S. Geological Survey, Professional Paper 830, 36 pp.

Shipton, Z. K., & Cowie, P. A. (2001). Damage zone and slip-surface evolution over μm to km scales in high-porosity Navajo sandstone, Utah. Journal of Structural Geology, 23(12), 1825-1844.

Shipton, Z. K., Evans, J. P., & Thompson, L. B. (2005). The geometry and thickness of deformation-band fault core and its influence on sealing characteristics of deformation-band fault zones, in Sorkhabi R. and Tsuji Y., eds., Faults, fluid flow, and petroleum traps: American Association of Petroleum Geologists Memoir 85., v. 85, p. 181–195, doi:10.1306/1033723M853135.

Sibson, R. H. (1992). Implications of fault-valve behaviour for rupture nucleation and recurrence. Tectonophysics, 211(1-4), 283-293.

Sigda, J.M., Wilson, J.L., 2003. Are faults preferential flow paths through semiarid and arid vadose zones? Water Resour. Res. 39 (8), 1225. http://dx.doi.org/10.1029/2002WR001406.

Soden, A.M., Shipton, Z.K., 2013. Dilational fault zone architecture in a welded ignimbrite: the importance of mechanical stratigraphy. J. Struct. Geol. 51, 156–166.

Soliva, R., Schultz, R. A., Ballas, G., Taboada, A., Wibberley, C., Saillet, E., & Benedicto, A. (2013). A model of strain localization in porous sandstone as a function of tectonic setting, burial and material properties; new insight from Provence (southern France). *Journal of Structural Geology*, *49*, 50-63.

Sonder, R. A. (1924). Zur Geologie and Petrographie der Inselgruppe yon Milos. Zeitschr. Volc, 8, 11-231.

Steefel C. I. and van Cappellen P. 1990. A new kinetic approach to modeling water-rock interaction: The role of nucleation, precursors and Ostwald ripening. Geochimica et Cosmochimica Acta 54, 2657–2677.

Stewart, A. L. (2003). Volcanic facies architecture and evolution of Milos, Greece (Doctoral dissertation, University of Tasmania).

Stewart, A. L., & McPhie, J. (2003). Internal structure and emplacement of an Upper Pliocene dacite cryptodome, Milos Island, Greece. Journal of Volcanology and Geothermal Research, 124(1-2), 129-148.

Tibaldi, A., Pasquare, F.A., Papanikolaou, D. and Nomikou, P., 2008. Tectonics of Nisyros Island, Greece, by field and offshore data, and analogue modelling, Journal of Structural Geology 30, 1489-150.

Torabi, A., Aydin, A., Cilona, B.E., Deng, J.S., 2015. The dynamics and interaction of compaction bands in Valley of Fire State Park, Nevada (USA): implications for their growth, evolution, and geostatistical property. Tectonophysics 657, 113–128.

Tschegg C., Hou Z., Rice A. H. N., Fendrych J., Matiasek E., Berger T. and Grasemann B. 2020. Fault zone structures and strain localization in

clinoptilolite-tuff (Nižný Hrabovec, Slovak Republic). Journal of Structural Geology 138, 104090.

Van Hinsbergen, D. J. J., Snel, E., Garstman, S. A., Marunţeanu, M., Langereis, C. G., Wortel, M. J. R., and Meulenkamp, J. E., 2004, Vertical motions in the Aegean volcanic arc: Evidence for rapid subsidence preceding volcanic activity on Milos and Aegina, Mar. Geol., 209, 329–345, https://doi.org/10.1016/j.margeo.2004.06.006.

White A. F. 1983. Surface chemistry and dissolution kinetics of glassy rocks at 25°C. Geochimica et Cosmochimica Acta Vol. 47, pp. 803-815.

Wilson, J.E., Goodwin, L.B., Lewis, C.J., 2003. Deformation bands in nonwelded ignimbrites: petrophysical controls on fault-zone deformation and evidence of preferential fluid flow. Geology 31, 837–840.

Wilson J. E, Goodwin L. B. and Lewis C. 2006. Diagenesis of deformation band faults: Record and mechanical consequences of vadose zone flow and transport in the Bandelier Tuff, Los Alamos, New Mexico. Journal of Geophysical Research 111, B09221.

Wong, T.F., David, C., Zhu, W., 1997. The transition from brittle faulting to cataclastic flow in porous sandstones: mechanical deformation. J. Geophys. Res. 102, 3009–3025.

Yielding, G. (2002). Shale gouge ratio—Calibration by geohistory. In Norwegian petroleum society special publications (Vol. 11, pp. 1-15). Elsevier.

Zhu, W., Baud, P., Vinciguerra, S., Wong, T.-F., 2011. Microtectonics of brittle faulting and cataclastic flow in Alban Hills tuff. J. Geophys. Res. 166, B06209. http://dx.doi.org/10.1029/2010JB008046.

Zou, C., 2013. Volcanics Reservoirs in Petroleum Exploration, first ed. Elsevier, Beijing, China 204pp.

Zhou, X., Kuiper, K., Wijbrans, J., Boehm, K., and Vroon, P. (2021). Eruptive history and 40 Ar⁄ 39 Ar geochronology of the Milos volcanic field, Greece. Geochronology, 3(1), 273-297.

Figures

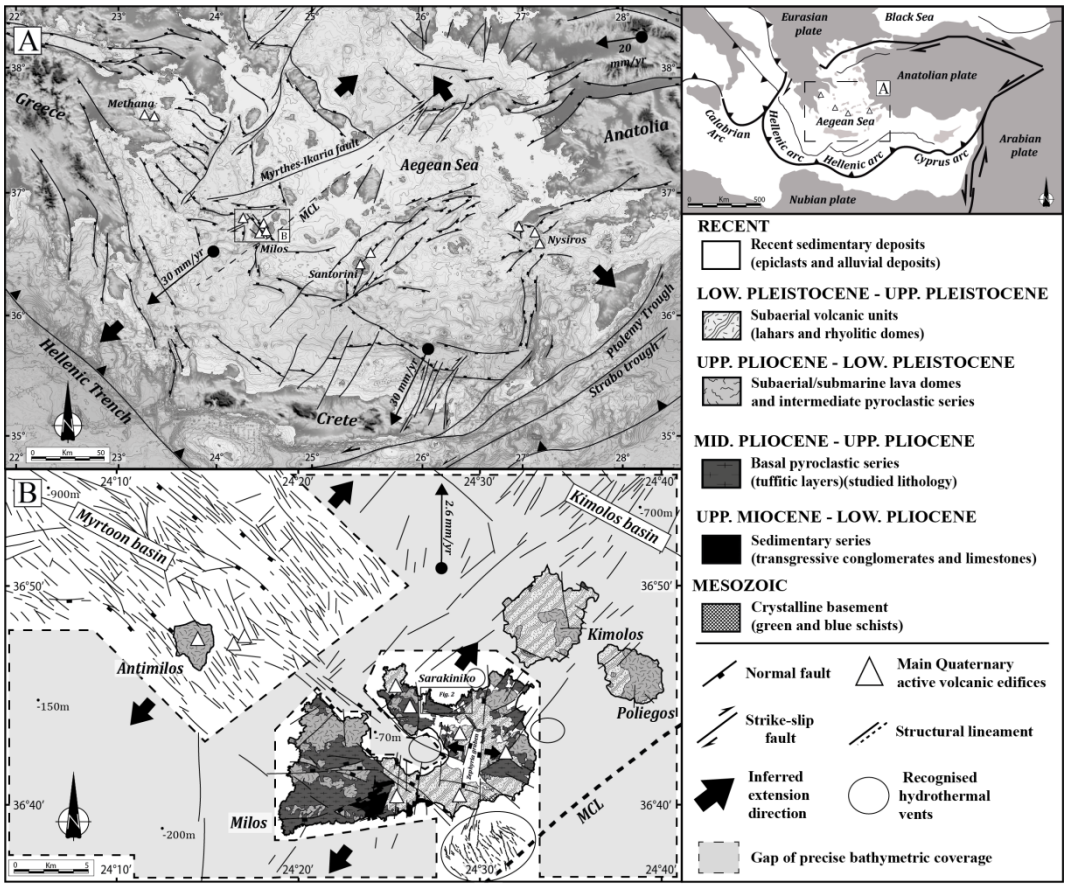

Figure 1: (A) Structural map of the South Aegean region showing the main volcanic centers and the main faults/structural lineaments. The structural mapping is based on published work by Gautiez *et al.* (1993), Tibaldi *et al.* (2008), Pavlides *et al.* (2009), Nomikou *et al.* (2013), Tsampouraki *et al.* (2015,2021) and Sakellariou *et al.* (2016). MCL: Mid-Cycladic Lineament. (B) Structural sketch of the Milos Archipelago showing the multi-direction interacting volcanic rift systems. The onshore structural sketch is based on work by Fytikas (1977, 1989). The offshore structural mapping is based on the bathymetry published in Nomikou et al. (2013). The poor quality of bathymetric data between the Myrtoon basin and the Milos Island explains the lack of accuracy of the structural mapping in this area.

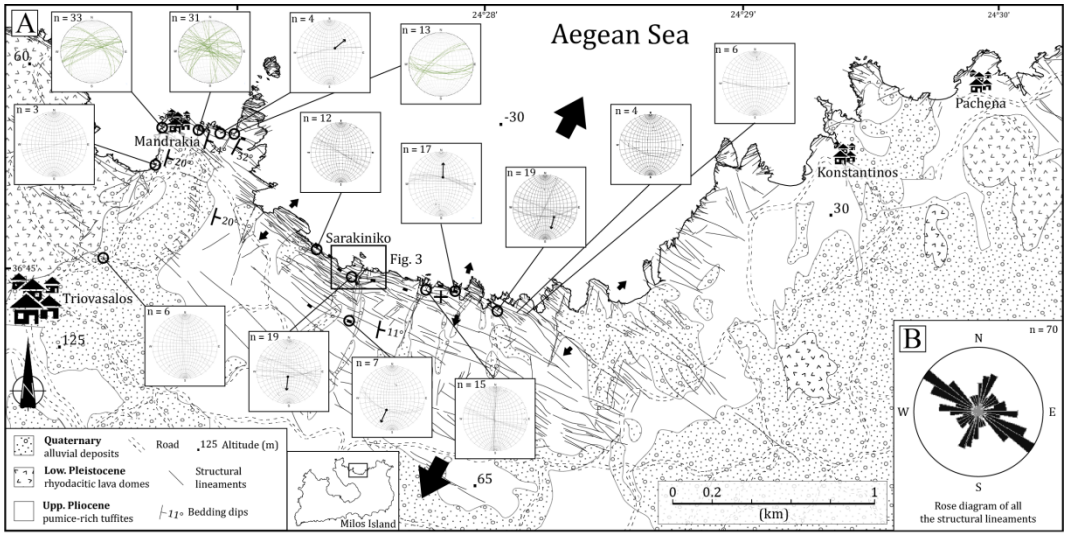

Figure 2: (A) Structural sketch of the Sarakiniko study area highlighting the main structural lineaments based on aerial images (Google Earth, CNES – AIRBUS, July 2013) and the stereoplots of faults, Dbs and fractures from field work. Displayed lithologies are based on work by Fytikas (1977). (B) Rose diagram displaying all structural data of lineaments along the northern coast of Milos. Data are represented as vertical fractures for synthetic purposes. The chronology of deformation is given in the text (section 4.1.) and is sketched in Figure 3b.

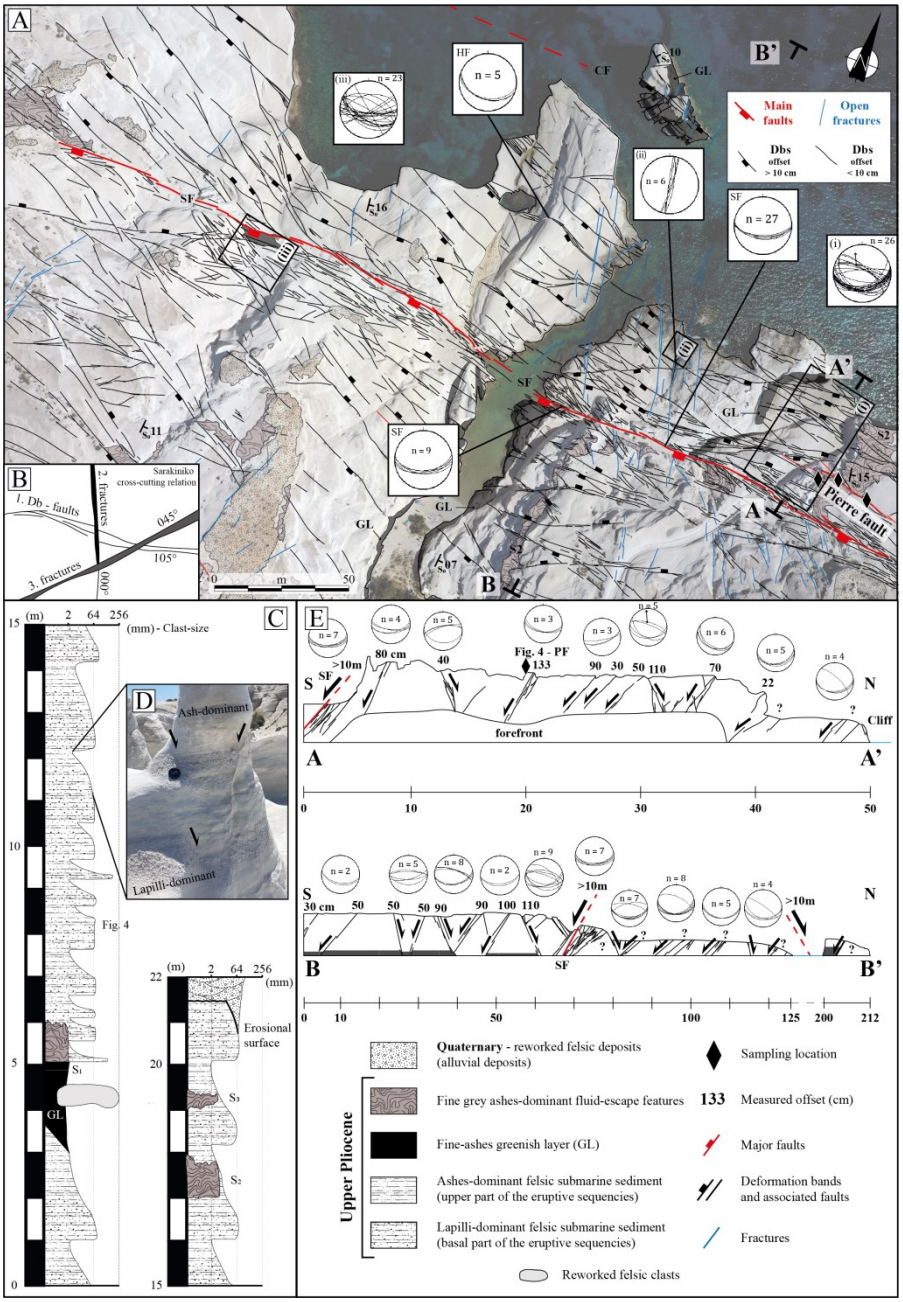

Figure 3: (A) Structural sketch of the Sarakiniko area showing the main structural lineaments based on drone imagery. Stereoplots are given for faults, Dbs and fractures based on typology inferred from fieldwork. (B) Representative example of the observed cross-cutting relationships between (i) E-W trending Deformation Bands (Dbs), (ii) N-S fractures and (iii) 045-trending fractures (cf Section 4.1 in the text). (C) Sedimentological log of the Sarakiniko Canyon studied succession. (D) Outcrop picture showing the undeformed tuffs (host rock). (E) North-South trending structural cross-sections of the study area displaying the measured offsets in cm. The cross-sections layouts are displayed on A. Orientation of structures (i.e. Dbs, fractures, faults) are given in the equal-area and lower hemisphere projections. The images in Figure 3a were captured in 2019 using a DJI Mavic 2 Pro equipped with a Hasselblad L1D-20 camera.

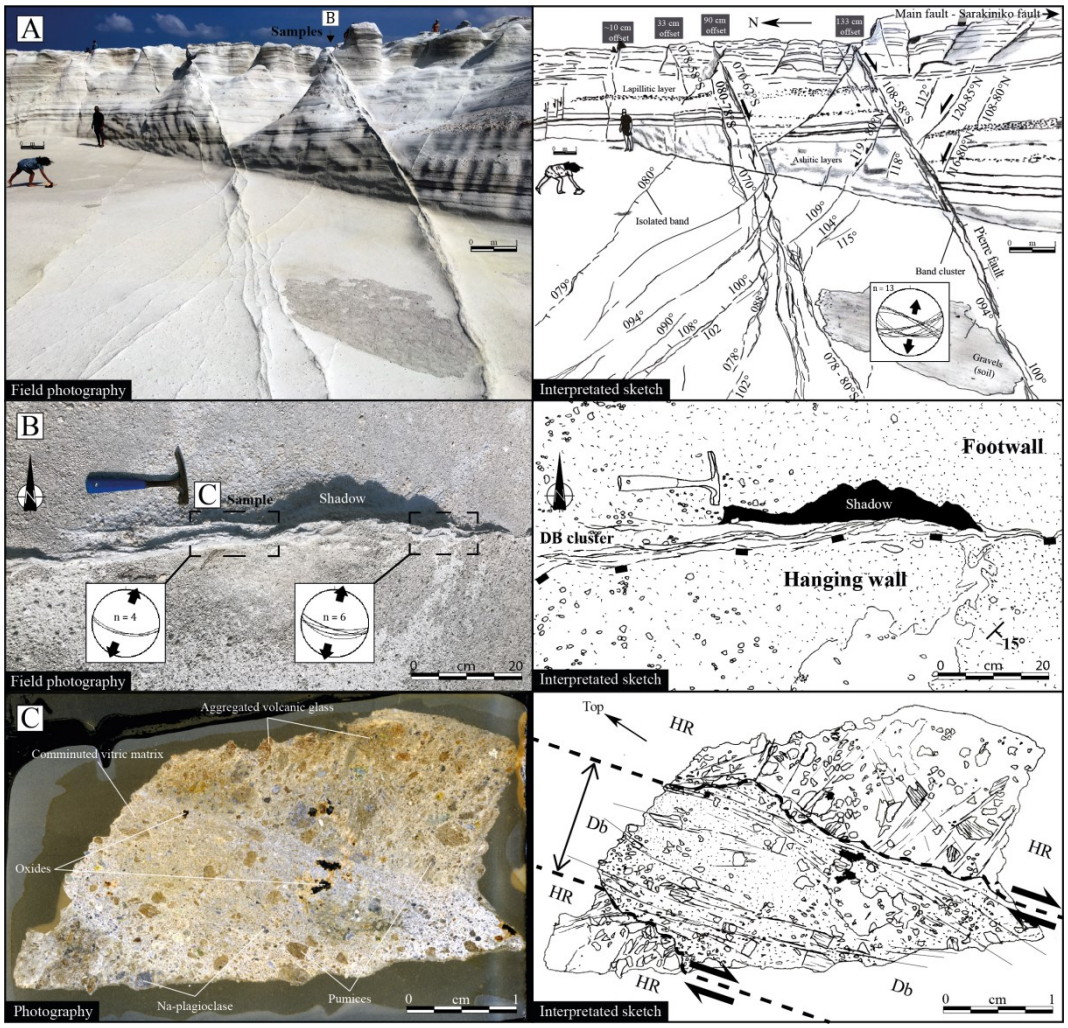

Figure 4: (A) Outcrop picture of the studied DBs network (Pierre fault) and associated structural interpretation and stereoplot data. (B) Outcrop picture, structural data and structural interpretation showing the Dbs cluster sampled in this study. (C) Sample-scale details of the Db and related structural interpretation. Both intragranular and transgranular fracturing are recognized in the Db, which is accordingly typified by grain-size reduction compared to the host-rock (HR).

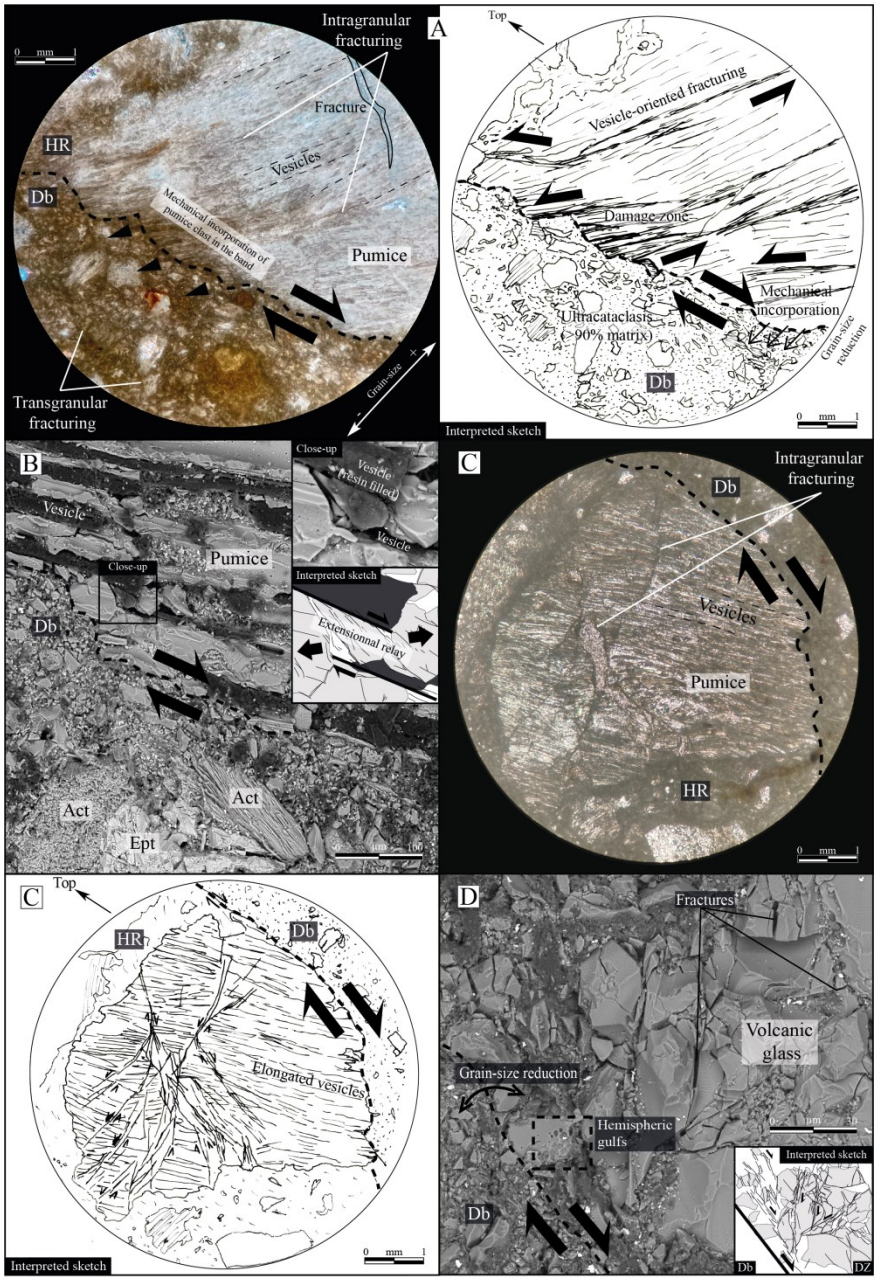

Figure 5: Microstructural observations of Dbs (A) Plane-polarized light optical microscope image (left) and corresponding sketch (right) of a pumice clast located at the DB vicinity (damage zone). The drastic grain-size contrast highlights a sharp transition between the host-rock (HR) and the Db. Db damage zone is expressed by fractures sub-parallel to the elongated vesicles of the pumice. (B) SEM image of fractures and shearing along fractures into a pumice fragment at the vicinity of a DB. The fractures are preferentially localized along the pumice vesicles. An extensional relay between two slip surfaces individualizes a 10-µm scale glass clast. (C) Plane-polarized light optical microscope image (second row; right) of a pumice located at the Db/host-rock transition and corresponding sketch (third row; left). Intra-granular fracturing develops sub-perpendicularly to the elongated vesicles. (D) SEM image of non-vesiculated volcanic glass showing both intra-granular and transgranular fracturing. Glass comminution and fracture growth lead to a drastic grain-size reduction.

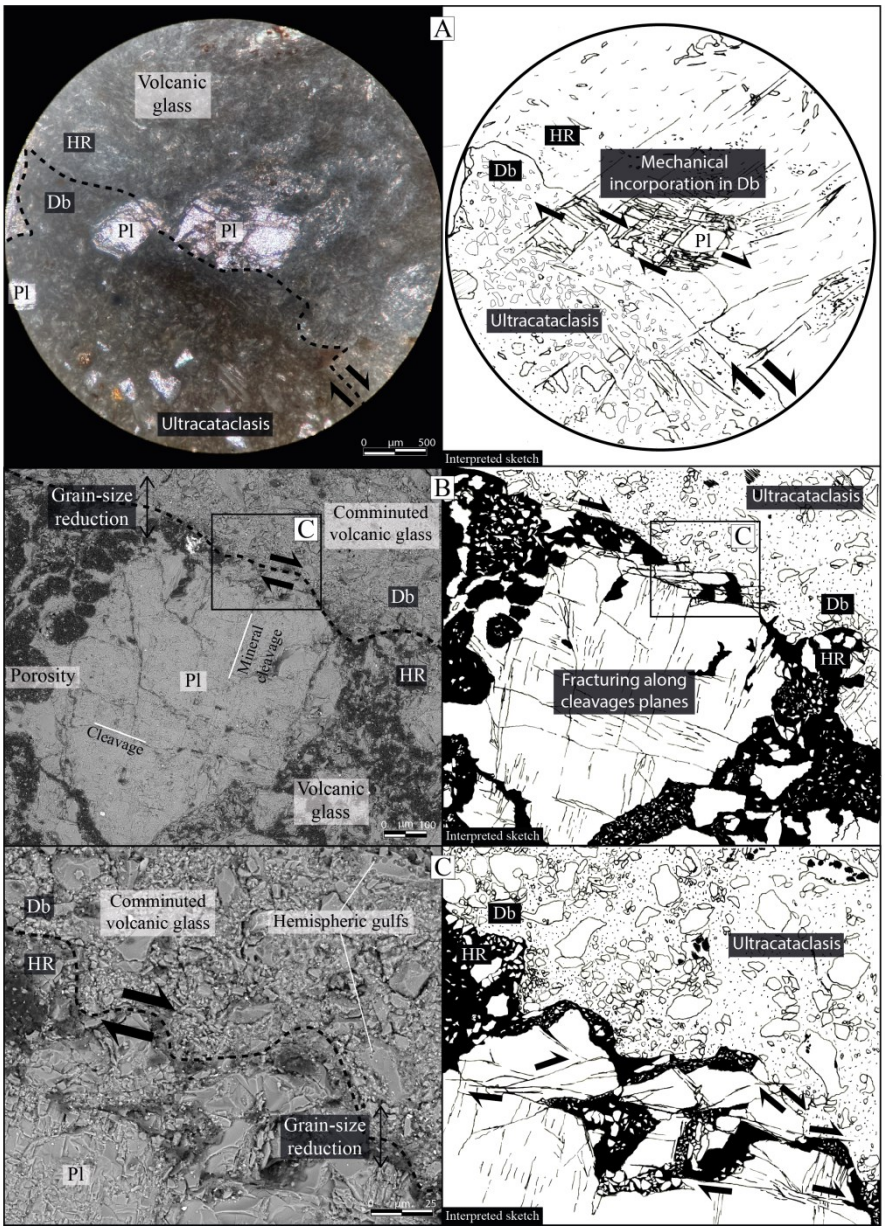

Figure 6: Mechanical deformation related to Db development. (A) Optical microscope image (cross-polarized light) (left) and corresponding sketch (right) showing fractured plagioclases (Pl) at the transition between a Db and the HR. Intra and transgranular fracture development leads to mineral comminution, grain-size reduction and therefore cataclasis. The cataclastic grains appear to be mechanically incorporated into the Db. (B) SEM image (left) and corresponding sketch (right) of a plagioclase (Pl) crystal at the HR/Db transition. The interpreted sketch shows two crystallographic cleavages representing likely mechanical weaknesses *i.e.* fracture planes. (C) SEM image (left) and corresponding sketch (right) showing deformation of a plagioclase at the HR/Db contact. Fracture intensity, length and connectivity increase towards the Db. Note that mineralogical cleavages are also used by the mechanical deformation and localize shearing.

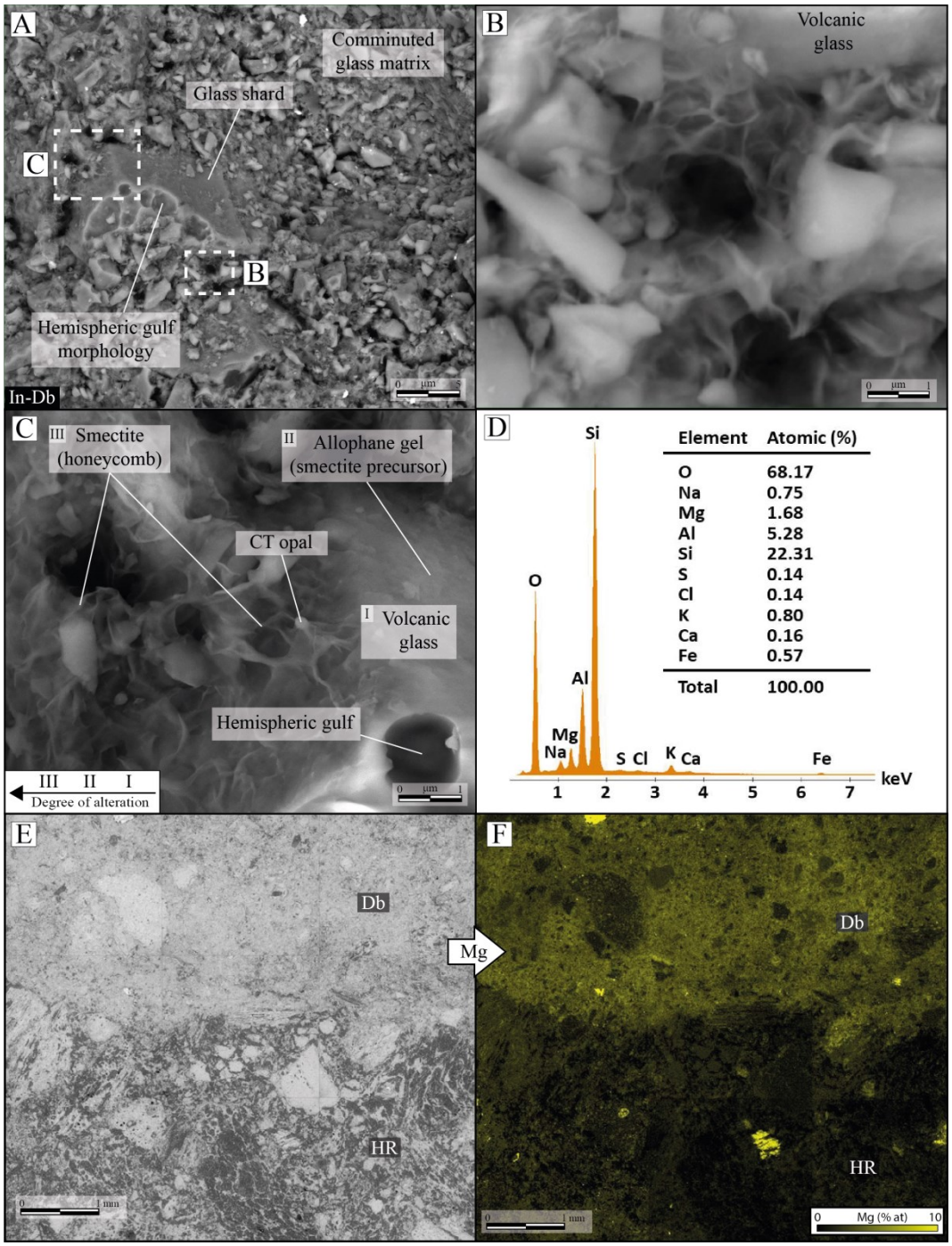

Figure 7: SEM and X-EDS local analysis of altered local zones in relation to fluid-rock interaction. (A) SEM image of volcanic glass comminuted fragments in deformation band displaying hemispheric gulfs which may be interpreted as evidence of dissolution. (B) Close-up view Fig. 7a) on honeycomb-shaped material interpreted as smectite filling the interclast (intergranular) porosity. (C) Close-up on honeycomb-shaped material coating a volcanic glass and interpreted as smectite (see D). The smectite seems to form at the expense of the volcanic glass (through a precursor phase of likely allophane composition; Christidis, 2001). The small spherules are opal-CT representing diagenetic byproducts

formed by co-precipitation of silica during the neoformation of smectites (see (D) (Christidis, 2001). (D) Local EDS spectrum measured on Fig. 7c and associated ZAF atomic (%) quantification. These EDS data can be *structurally* interpreted as a mix of 70 % of $(Na, K, Ca)_{0.4}\ (Al, Mg, Fe)_2\ Si_4\ O_{10}(OH)_2$ (which is essentially compatible with the stoichiometry of a generic dioctahedral smectite) and 30 % of $SiO_2.H_2O$ (opal-CT) along with traces of halite[3]. This structural interpretation *at the first order*[4] may be tentatively refined by considering that smectite is partially illitized, consistently with previous findings in Milos Island e.g. Christidis and Dunham (1993). This is supported by the EDS data in (D) which are fully consistent with a threefold *structural* interpretation: a mix of 50 % of a Montmorillonite type smectite *i.e.* $(Na, Ca)_{0.3}\ (Al, Mg)_2\ Si_4\ O_{10}(OH)_2$, 15 % of illite (here $K\ Al_2\ (Al\ Si_3)\ O_{10}(OH)_2$) and 35 % of hydrated siliceous $SiO_2.H_2O$. (E) SEM image showing a Db/HR boundary and (F) X-EDS chemical mapping (At%) showing a marked Mg-enrichment in the Db with a preferential localization of Mg-rich minerals in intergranular spaces. Note that the bright grains (Mg-rich) in the Mg EDS mapping (F) are orthopyroxenes present in the Db and in the HR.

[3] In order to unmix the mixture (*i.e.* in order to assess a lower bound of the relative fraction of the siliceous phase in the mixture), we considered as an approximation that Al is essentially 6-coordinated in the phyllite component of the mixture.

[4] There is a slight excess of interlayer cations in the phyllite within in this chemical interpretation of the EDS data.

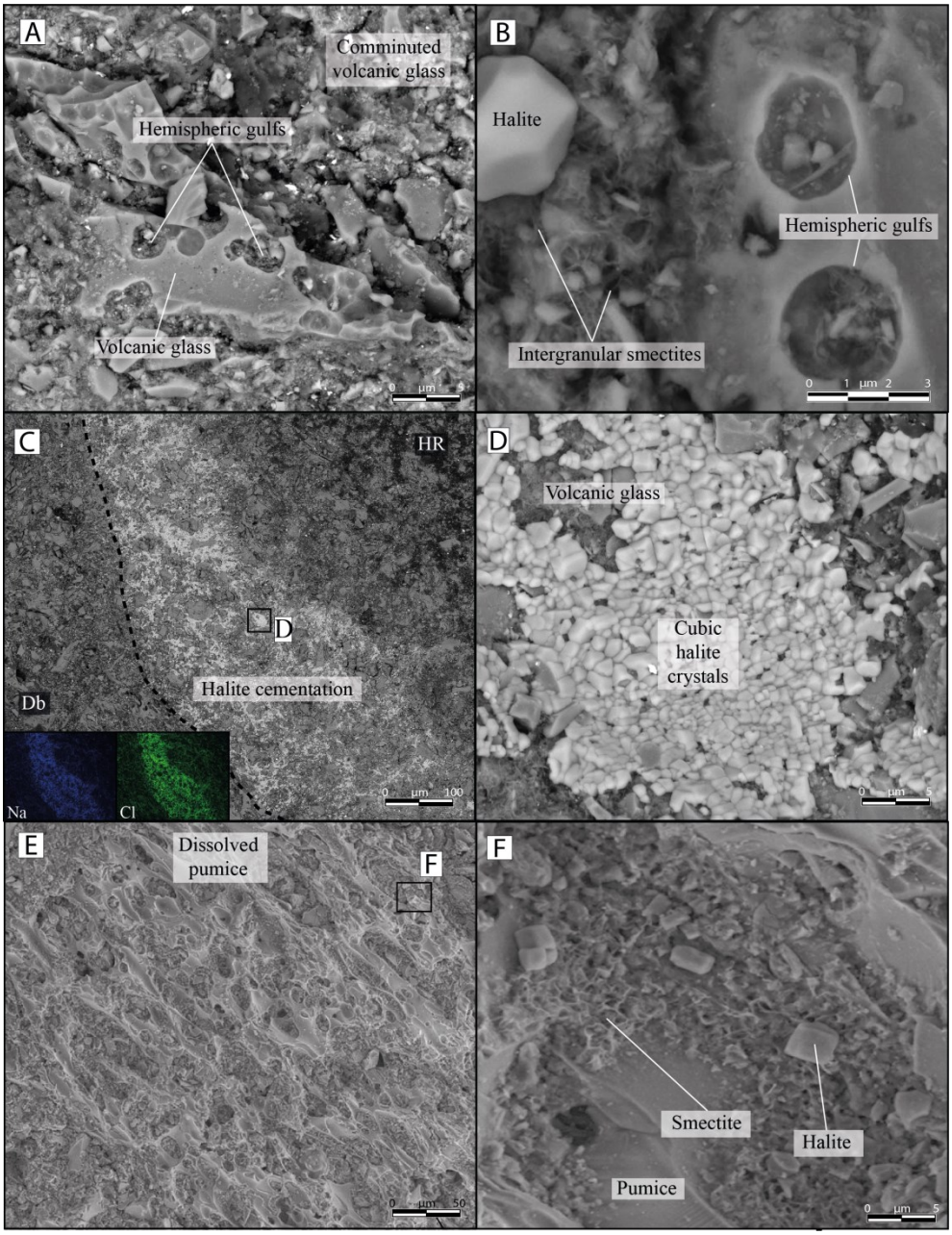

Figure 8: SEM images of altered local zones in relation to fluid-rock interaction. (A) Comminuted volcanic glass fragments within a Db showing corrosion. (B) Detailed view within a Db showing neoformed smectite filling the intergranular porosity and corrosion gulfs on a volcanic glass grain. The floor of one gulf shows a discrete trace of smectite. Note the presence of a halite grain in the Db. (C) HR/Db transition where halite cementation has been unambiguously identified by X-EDS chemical mapping (lower left inset). This mineralization is located along the HR/Db transition within the host porous tuff (HR side). (D) Details of the halite cementation. Halite crystals display an undeformed cubic-like crystal shape suggesting a post-Db cementation. (E) and (F) Alteration of a sub-mm porous pumice located in between Db strands (damaged zone). The pumice is highly dissolved and coated by smectite.

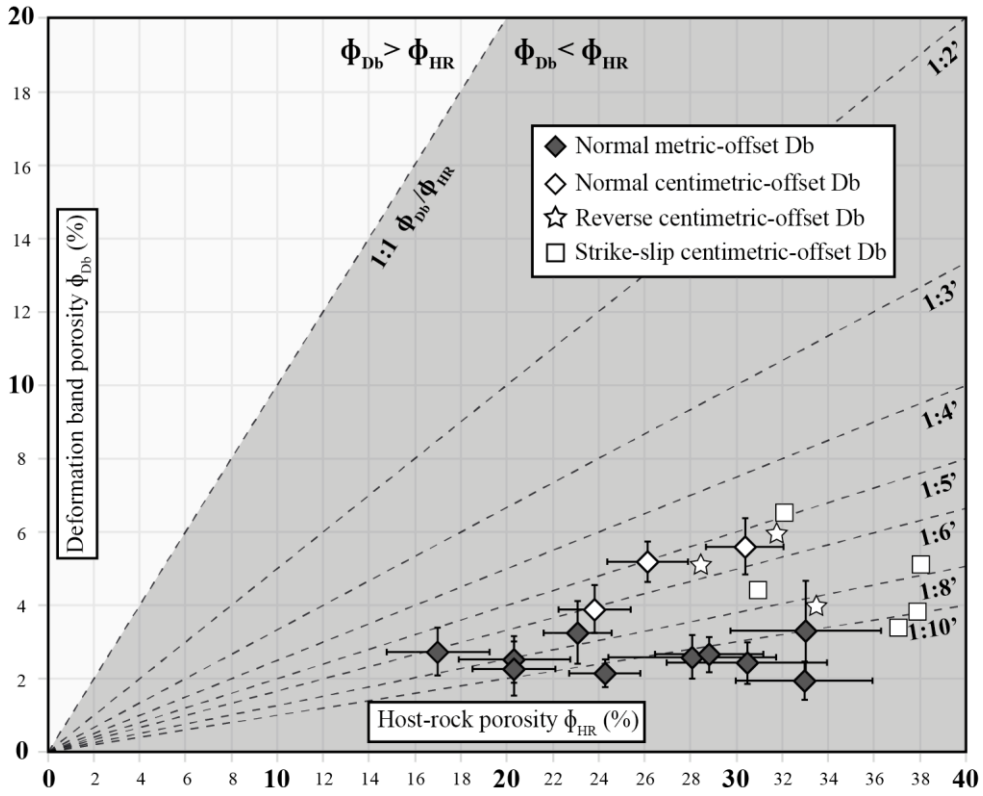

Figure 9: Plot of measured porosity (ϕ) values, displaying Db porosity versus HR porosity values at Sarakiniko. The darker area is associated with a reduction of porosity in the Db relative to HR. Reduction factor lines are displayed to ease the quantitative reading of the plot. Each point for Sarakiniko corresponds to the mean value of ϕ_{Db}/ϕ_{HR} along a sub centimetric-wide band normal to the Db/HR boundary. Error bars are calculated as errors on the average i.e. $\frac{\sigma}{\sqrt{N}}$ where N is the number of porosity measurements in a sample and σ is the standard deviation (which characterizes the dispersion around the average). Data for reverse and strike-slip Dbs are taken from Cavailhes and Rotevatn (2018).

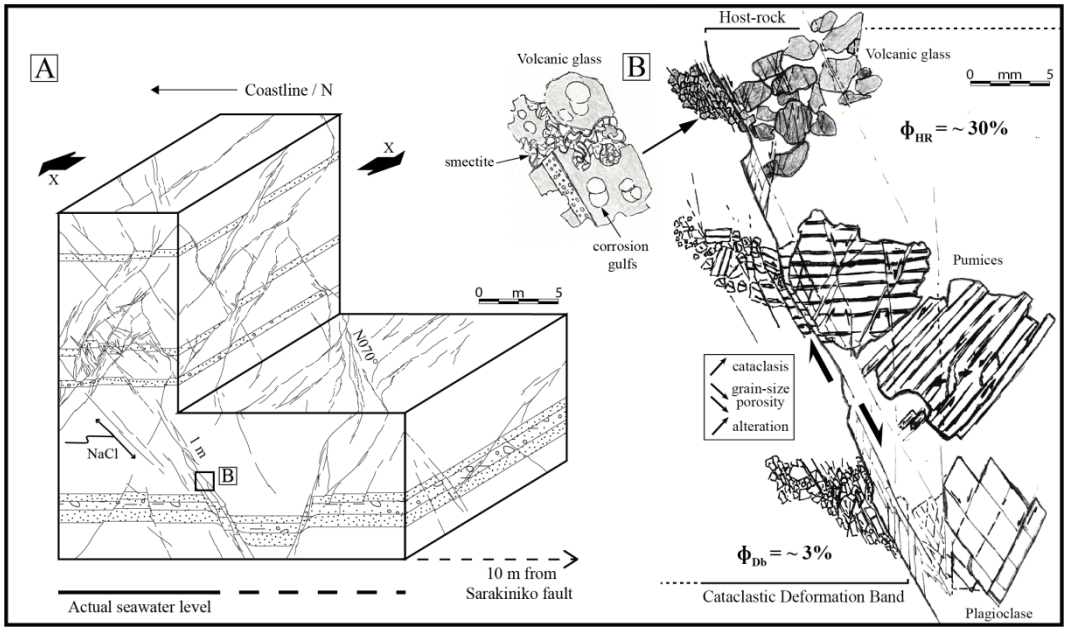

Figure 10: (A) Present-day 10-m scale architecture of the NCSBs network affecting the studied porous volcaniclastic tuffs under an extensional tectonic regime. NCSBs are interpreted as a background deformation despite the presence of the 10 m-displacement Sarakiniko fault. (B) Synoptic sketch of the observed structures, the inferred deformation mechanisms and related fluid-rock interactions. Cataclasis development seems to be promoted where the HR shows lowered mechanical properties *e.g.* pumice elongated vesicles or mineral cleavages. Smectites are preferentially observed within the Dbs which are typified by a higher fresh reactional surface due to enhanced cataclasis. The dissolution of the unstable volcanic glass into the NCSBs probably leads to smectite neoformation. Undeformed halite mineralizations are present locally along the HR/Db boundary. This may support that seawater flow responsible for this mineralization postdates Dbs formation. This observation may also suggest that Dbs also act as a permeability barrier for fluid-flow at the dm-scale after self-sealing takes place.

Appendix A. Supplementary material

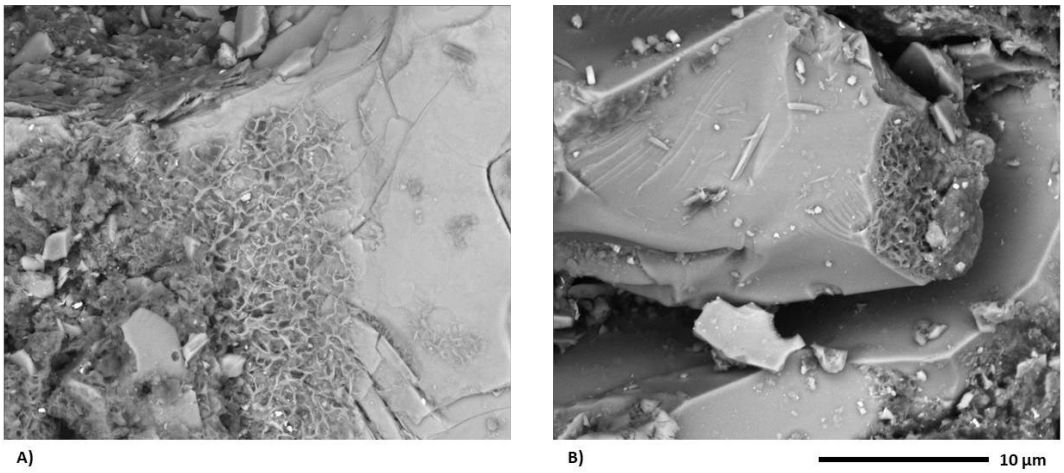

Figure A1. SEM micrographs of the HR illustrating occasional plates of neoformed smectites coating volcanic glass grains (Fig. A1.A) and/or fresh reactive surfaces (Fig. A1.B).

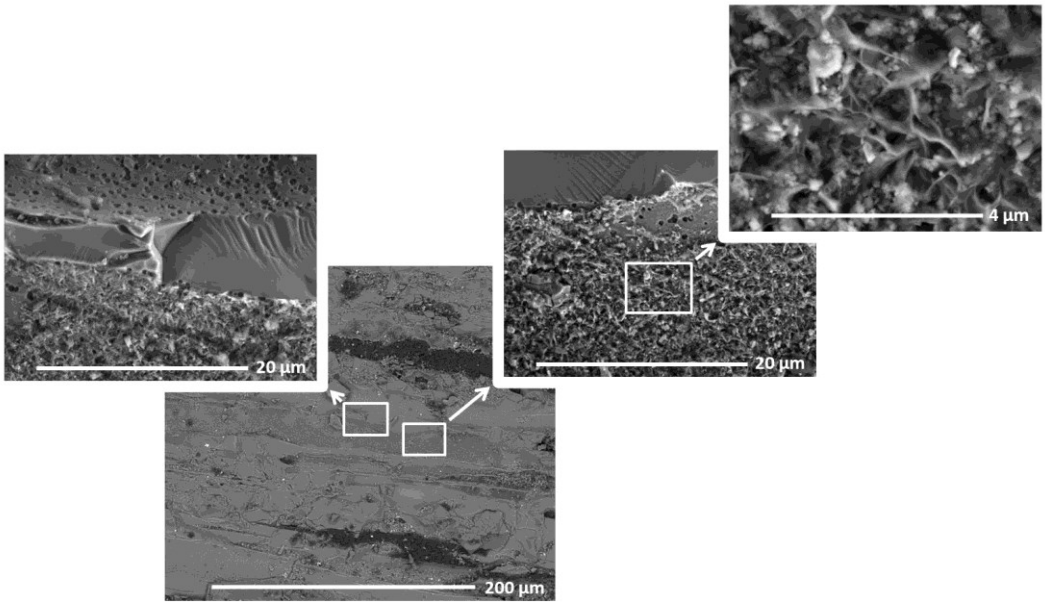

Figure A2. SEM micrographs within a single strand Db illustrating the alteration of a sub-mm porous pumice showing plentiful corrosion gulfs (clear evidence of enhanced fluid fluxes episodes that typify Dbs) and occurrence of pore-lining smectites (more typical in this study of HR porosity dimensions and water to rock ratio (Fig. A1).